Cell

Natural Neural Projection Dynamics Underlying Social Behavior

Lisa A. Gunaydin,[1,5] Logan Grosenick,[1,2,5] Joel C. Finkelstein,[1,5] Isaac V. Kauvar,[1,5] Lief E. Fenno,[1,2] Avishek Adhikari,[1] Stephan Lammel,[3] Julie J. Mirzabekov,[1] Raag D. Airan,[1] Kelly A. Zalocusky,[1,2] Kay M. Tye,[1] Polina Anikeeva,[1] Robert C. Malenka,[3] and Karl Deisseroth[1,3,4,*]
[1]Department of Bioengineering
[2]Neuroscience Program
[3]Department of Psychiatry and Behavioral Sciences
[4]Howard Hughes Medical Institute
Stanford University, Stanford, CA 94305, USA
[5]Co-first author
*Correspondence: deissero@stanford.edu
http://dx.doi.org/10.1016/j.cell.2014.05.017

SUMMARY

Social interaction is a complex behavior essential for many species and is impaired in major neuropsychiatric disorders. Pharmacological studies have implicated certain neurotransmitter systems in social behavior, but circuit-level understanding of endogenous neural activity during social interaction is lacking. We therefore developed and applied a new methodology, termed fiber photometry, to optically record natural neural activity in genetically and connectivity-defined projections to elucidate the real-time role of specified pathways in mammalian behavior. Fiber photometry revealed that activity dynamics of a ventral tegmental area (VTA)-to-nucleus accumbens (NAc) projection could encode and predict key features of social, but not novel object, interaction. Consistent with this observation, optogenetic control of cells specifically contributing to this projection was sufficient to modulate social behavior, which was mediated by type 1 dopamine receptor signaling downstream in the NAc. Direct observation of deep projection-specific activity in this way captures a fundamental and previously inaccessible dimension of mammalian circuit dynamics.

INTRODUCTION

Impaired social interaction is a hallmark of several psychiatric disorders, including autism, schizophrenia, depression, and social anxiety disorder. In rodents, most studies on social behavior have focused on socio-sexual behaviors, such as pair bonding and behaviors related to sexual competition (Aragona et al., 2006; Curtis and Wang, 2005; Gingrich et al., 2000; Leypold et al., 2002; Liu and Wang, 2003; Young et al., 2001; Young and Wang, 2004). However, comparatively little is known about neural circuitry regulating adult same-sex, nonaggressive social interaction, which is of potential relevance for understanding circuits that go awry in social-function disorders (Silva and Ehninger, 2009).

Pioneering studies have implicated the neuromodulator dopamine (DA) in same-sex affiliative interactions (Puglisi-Allegra and Cabib, 1997; Robinson et al., 2002; Robinson et al., 2011). DA neurons in the VTA are involved in processing emotionally salient stimuli of both positive and negative valence. The VTA is a heterogeneous region comprised of diverse cell types that may play distinct roles in modulating reward and aversion based on connectivity to different upstream and downstream structures (Brischoux et al., 2009; Budygin et al., 2012; Chaudhury et al., 2013; Kalivas and Nakamura, 1999; Lammel et al., 2011, 2012; Mirenowicz and Schultz, 1996; Tye et al., 2013). These cells project broadly throughout the brain to limbic regions such as the medial prefrontal cortex (mPFC), NAc, and amygdala, structures that may mediate both appetitive and aversive processes. However, it is unknown which if any of these projections might play a causal role in driving or inhibiting social behaviors. Moreover, in general, the real-time neural circuit dynamics causally involved in social behavior remain poorly understood, and the large number of downstream VTA targets and postsynaptic DA receptors together point to the need for new tools that allow observation of targeted cell types and their projections during naturalistic conditions and perturbation of activity in a downstream receptor and region-specific manner.

We approached this challenge by developing optical tools to selectively observe and control specific VTA circuit elements, projections, and downstream targets on a timescale relevant to social interaction. First, we sought to develop a recording technique sensitive enough to track real-time dynamics of genetically and topologically specified subsets of neuronal projections in freely moving mice, using novel photometric devices together with genetically encoded Ca^{2+} indicators (Akerboom et al., 2012; Chen et al., 2013) for direct in vivo measurement of a previously inaccessible variable: the coordinated activity of neuronal afferents projecting to a particular downstream target deep in the brain of a behaving mammal. We next applied this method to determine quantitative features of projection-specific dynamics during behavior to identify circuit elements predictive

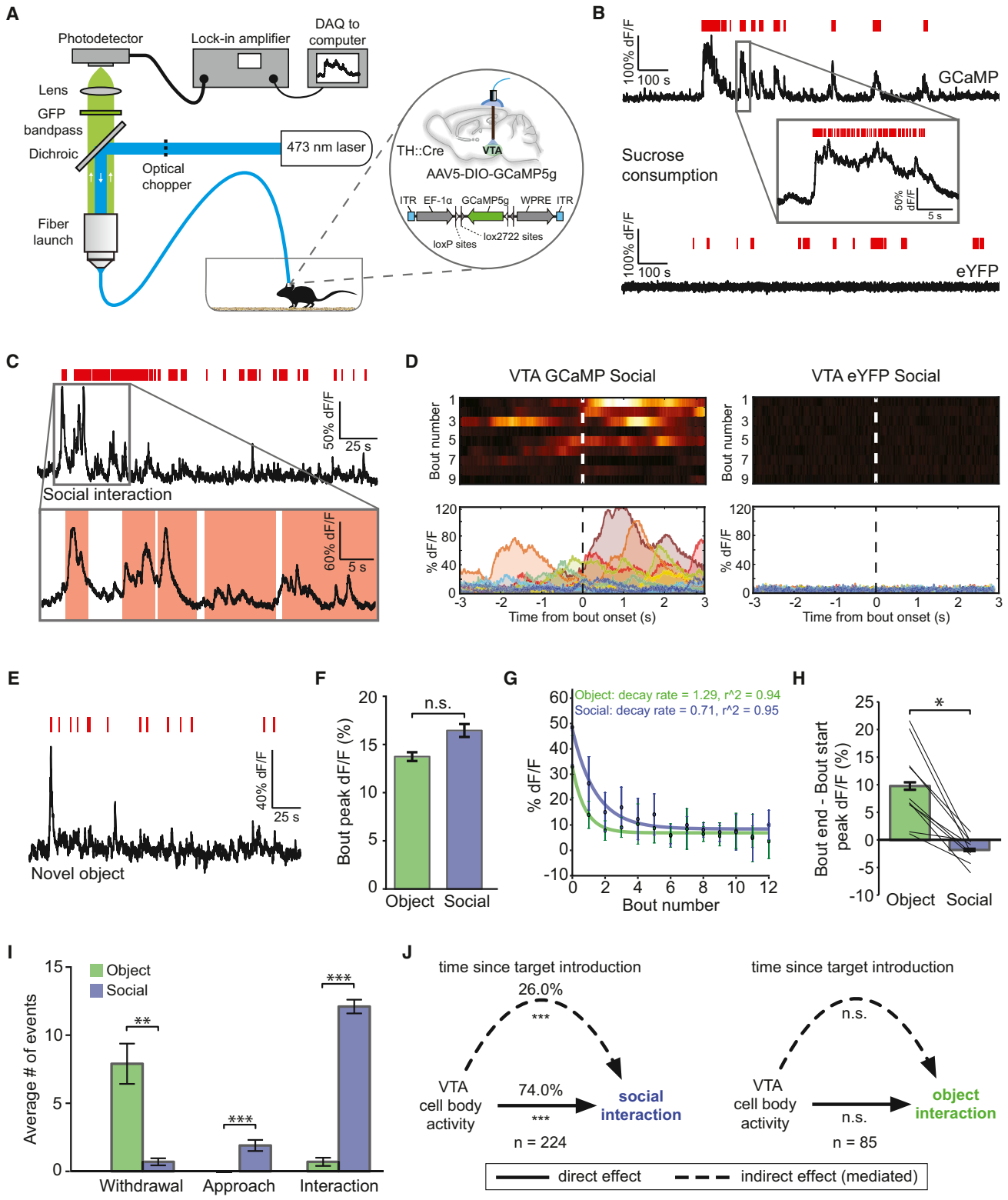

Figure 1. Fiber Photometry of Neural Dynamics during Social Interaction

(A) (Left) Photometry setup. Light path for fluorescence excitation and emission is through a single 400 μm fiber optic implanted in VTA. (Right) Viral targeting of GCaMP5 to VTA-DA neurons.

(legend continued on next page)

of social interactions. Complementing observation of these natural behaviorally evoked activity patterns, we employed optogenetic tools to define causal roles of these same projections (relative to other pathways) in modulating social behavior. And finally, we engineered a light-activated postsynaptic neurotransmitter receptor to test the causal sufficiency of DA receptor signaling at the identified projection target for social behavior modulation. Together, these investigations provide insight into natural and causal circuit dynamics underlying social behavior modulation and illustrate an approach for testing the behavioral relevance of circuits characterized by cell location, type, projection target, and target receptor during behavior.

RESULTS

Optical Detection of Reward-Related VTA Ca^{2+} Signals in Freely Moving Animals

Fast-scan cyclic voltammetry has revealed DA changes in striatal regions that correlate with bouts of social interaction (Robinson et al., 2002, 2011). However, causality and specificity for cells or projections in driving social interaction have been unknown, and there have been no recordings of identified DA neurons or their projections during any social paradigm. To observe the real-time activity of specified neural projections in complex behaviors, we developed a novel technique: fiber photometry. Previous pioneering devices used either acutely placed multiple fiber optics to record genetically encoded Ca^{2+} signals in cell bodies of awake animals in striatum (Cui et al., 2013) or multimode fibers to record cell bodies in cortex (Lutcke et al., 2010; Schulz et al., 2012). We developed a design that was simple (only a single multimode optical fiber), suitable for recording from deep brain structures, and sensitive enough to detect activity changes not only in cell bodies, but also in axons during behavior, where signals are considerably smaller. This fiber photometry (light measurement with a single-fiber-optic device sensitive enough to detect activity in axonal fibers) relies on a lock-in amplifier and a high-sensitivity photoreceiver along with custom software to record (through an implanted 400 μm optical fiber) the population activity of neural circuit elements expressing a genetically encoded Ca^{2+} indicator (Figure 1A). The single fiber allows chronic, stable, minimally disruptive access to deep brain regions and interfaces with a flexible patch-cord on the skull surface. For cell-type-specific recording of Ca^{2+} transients—a proxy for certain neural activity (Akerboom et al., 2012)—we injected a Cre-dependent adeno-associated virus (AAV) carrying the GCaMP5g gene into the VTA of transgenic TH::Cre mice (henceforth referred to as TH-GCaMP; Figures 1A and S1A), and implanted an optical fiber in the VTA for simultaneous delivery of 473 nm excitation light and collection of GCaMP5g fluorescence emission. Activity-dependent fluorescence emitted by cells in the volume is collected simultaneously; after propagating back through the same patch-cord used to deliver excitation light, this fluorescence is spectrally separated using a dichroic, passed through a single band filter, and focused onto a photodetector (Figure 1A).

To first test whether this system was capable of detecting VTA activity in a temporally precise manner, we recorded Ca^{2+} signals in VTA neurons of TH-GCaMP mice given access to sucrose solution, an established natural reward. Sucrose consumption was assessed using a contact "lickometer," which registered an event every time the mouse completed a circuit from a metal spout to a metal operant chamber floor, time-locked to the Ca^{2+} recording. This setup enabled readout of VTA responses with temporal precision on the order of milliseconds. We observed a robust increase in VTA GCaMP fluorescence when mice licked for sucrose (average peak dF/F: 68.3% ± 13.2% SEM; average mean dF/F: 29.7% ± 8.9% SEM), an effect that was absent in control mice expressing eYFP (Figure 1B). VTA signals were tightly correlated in time with onset of licking bouts (Figure S1B) and habituated over recording epochs (Figure S1C). Although no driver-line or injection targeting is fully specific, together with previous validation of high-specificity Cre expression in TH neurons of lateral VTA in this TH::Cre mouse line (Tsai et al., 2009; Tye et al., 2013) and DA receptor blockade results presented below, these data suggest validity of fiber photometry for recording temporally precise behavior-related signals in the targeted population (here referred to as VTA-DA neurons).

Neural Activity that Encodes and Predicts Social Interaction

Next we applied fiber photometry during same-sex social interaction. We recorded from the VTA of female mice during

(B) Photometry traces from mice expressing eYFP (bottom) and GCaMP5g (top) in VTA during the sucrose lickometer test, showing robust increases in GCaMP fluorescence correlated with sucrose licking epochs (red dashes). dF/F represents change in fluorescence from median of the entire time series.
(C) (Top) Example trace of VTA-DA activity in social behavior. (Red dashes) Interaction bouts. (Bottom) Zoom-in of gray box from above relating VTA-DA GCaMP signal and social interaction (colored boxes).
(D) Example heatmaps (top) and peri-event plots (bottom) aligned to start of interaction for mice expressing GCaMP (left) or eYFP (right). (Heatmaps) Warmer colors indicate higher fluorescence signal; (peri-event plots) warmer colors represent earlier interaction bouts.
(E) VTA-DA activity in novel object investigation. (Red dashes) Interaction bouts.
(F) Average peak fluorescence over the first ten interaction bouts (16.4% dF/F: social; 13.7% dF/F: novel object; n = 10, Wilcoxon signed-rank test, p = 0.5).
(G) Signal changes across bouts: social (blue) and novel object (green).
(H) Signal changes within bouts; novel object peak responses occur closer to interaction-bout end than do social peak responses (n = 10 individual animals plotted, gray lines; difference of peaks over 0.5 s from bout-end and bout-start: −1.7% dF/F social versus 9.7% dF/F novel object; Wilcoxon signed-rank test: p = 0.0051).
(I) Specific behaviors during 1 s behavioral video clips centered around peak fluorescence within each bout. Peak during novel object investigation occurs predominantly in withdrawing from object (92%), whereas peak fluorescence during social interaction occurs in approach (14%) or active investigation (81%) (n = 10 animals, 15 bouts/animal).
(J) Directed graphical model of causal mediation analysis (Experimental Procedures); though time elapsed partially mediates effects of VTA-DA neuron activity on latency to social interaction only, the majority of effect was direct rather than mediated (74.0% average direct effect, 26.0% average indirect effect mediated by time elapsed; both $p < 0.0001$).
Error bars represent SEM. See also Figure S1.

home-cage social interaction, in which a novel social target mouse was introduced into the test mouse cage for a 5 min epoch, and video time-locked to the VTA GCaMP signal was collected. Upon introduction of the social target, we observed a marked increase in activity of the targeted VTA neurons during interaction with this novel mouse (Figure 1C). This activity habituated over the behavior epochs, with strongest activity occurring during earlier bouts of interaction (Figure 1D). Such activity was absent in the eYFP control, indicating that observed transients were Ca^{2+} signals and not motion artifacts (Figure 1D).

To dissociate social activity from general novelty-related activity, in separate trials we exposed test mice to a novel object placed in the home cage (counterbalanced with novel mouse exposure). Mice interacted more frequently with a stranger mouse than with a novel object (Kaplan-Meier estimate for latency to next interaction, log-rank test $p < 0.0001$). Nevertheless, VTA activity in response to the novel object (Figure 1E) resembled peak VTA activity during social interaction, with similar amplitude (mean peak dF/F during interaction: 16.4% ± 2.1% SEM for social, 13.7% ± 1.4% SEM for novel object, n = 10; Wilcoxon signed-rank test, p = 0.5; Figure 1F) and similar decay across interaction epochs (peak fluorescence fit to $Ae^{-kb} + c$: A = amplitude, k = decay rate, b = bout number, and c = offset; social: $k = 0.71$, $r^2 = 0.95$, novel object: $k = 1.29$, $r^2 = 0.94$; Figure 1G). However, whereas social VTA responses aligned well with onset of interaction, novel object responses aligned more significantly with termination of the interaction bout (peak fluorescence within 0.5 s from end of interaction – peak fluorescence within 0.5 s from start: −1.7% dF/F for social, 9.7% dF/F for novel object; n = 10 animals, Wilcoxon signed-rank test: p = 0.0051; Figure 1H and Movies S1 and S2), suggesting that VTA responses in these two behaviors could represent different information given distinct timing relative to interaction onset.

To more closely examine VTA representation of social and object interactions, we identified the peak fluorescence within each interaction epoch and segmented time-locked behavioral videos into 1 s clips centered upon the time of maximal VTA activity to assess specific actions when VTA activity was highest. Behavior during these 1 s segments was assigned a binary value for approach, withdrawal, or active investigation (contact). We found prominent differences in the distribution of these behaviors in the social compared to novel object setting; when fluorescence was highest, mice exhibited significantly more withdrawals from the target during novel object epochs compared to social epochs (Figure 1I; n = 10, Wilcoxon rank-sum test with continuity correction, p = 0.003). Conversely, peak fluorescence during social epochs was associated with significantly more approach behavior and active investigation than with novel object (Figure 1I; n = 10, Wilcoxon rank-sum test with continuity correction, p = 0.0007, p = 0.0001, respectively; see also Figure S1D). These data suggest that, for social interaction, peak activity in these cells encodes appetitive approach behaviors, whereas during novel object investigation, peak activity appears to encode withdrawal behaviors.

Given the reliable association between peak VTA activity and approach/investigation of social targets, we hypothesized that observed DA neuron activity during a particular interaction epoch might be meaningful to the animal in terms of modulating its subsequent social approach behavior. To test this hypothesis, we investigated whether magnitude of the VTA signal during one interaction bout would predict latency to engage in another social interaction bout. We employed prediction analysis, using peak Ca^{2+} activity (Experimental Procedures) during one interaction to predict latency to engage in the next interaction. A survival regression model appropriate for time-to-event data was used to predict latency to the next interaction as a function of three variables: (1) peak Ca^{2+} activity (log-transformed), (2) time since target introduction (to control for habituation unrelated to neural activity), and (3) animal identity (to control for interanimal differences). For social interactions, increased peak Ca^{2+} activity during the previous interaction predicted shorter latency to interact again ($Z = -5.21$, $p < 0.0001$), whereas time since target introduction predicted longer latency to interact ($Z = 5.29$, $p < 0.0001$; consistent with decreases in interaction over time typically observed in such data). However, peak Ca^{2+} activity did not predict reduced latency to novel object interactions but instead showed a less pronounced effect in the opposite direction (significantly predicting longer latencies to the next interaction: $Z = 1.19$, $p = 0.02$; with a trend toward effect of time elapsed: $Z = 0.475$, $p = 0.053$). These data together illuminate the real-time dynamics of VTA-DA neurons during social interaction, demonstrating that activity of these neurons can predict social and novel object interaction behavior on a trial-by-trial basis and that the direction of these predictions is opposite for the two types of interaction.

Prediction analysis suggested an important role for VTA-DA neuron activity in social interaction; however, because VTA-DA neuron activity and latency to social interaction are both correlated with time elapsed from target introduction, we sought to further confirm that this predictive capability of the native dynamics of DA neurons on behavior was not merely mediated by the parameter of time elapsed. We used causal mediation analysis (Imai et al., 2010) to take into account effects of time elapsed on both VTA activity and behavior, represented by a simple directed graphical model (Figure 1J and Experimental Procedures). If apparent effects of VTA-DA neuron activity on subsequent behavior were spurious and if time elapsed were the only causal contributing influence to observed changes in latency to engage in interaction, we would expect time elapsed to completely mediate the effect of VTA-DA activity on this behavior. We found that, whereas time elapsed partially mediated effects of VTA-DA neuron activity on latency to social interaction, the majority of the effect of VTA-DA neuron activity was direct rather than mediated (Figure 1J; 74.0% average direct effect, 26.0% average indirect effect mediated by time elapsed; both $p < 0.0001$). In contrast, a similar mediation analysis on novel object interactions did not show significant direct or indirect effects of VTA-DA neuron activity on latency to interact (Figure 1J). Together, these fiber photometry results indicate that native VTA-DA neural activity both encodes and predicts social interaction and suggest that endogenous VTA dynamics may have a direct effect on social approach behavior.

Direct Control of VTA-DA Cells Bidirectionally Modulates Social Behavior

If VTA-DA activity peaks were causally involved in initiating or maintaining social interaction, then experimentally providing

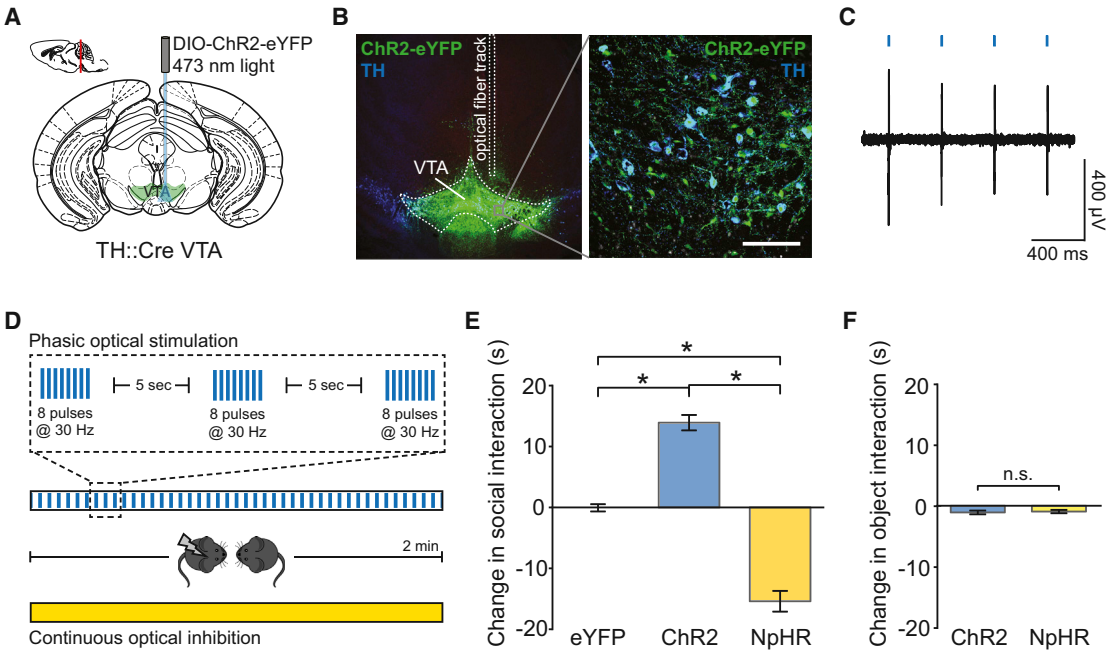

Figure 2. VTA Modulation of Social Behavior

(A) Injection of AAV5-DIO-ChR2 into VTA of TH::Cre mice.

(B) Confocal image: ChR2-eYFP expression in VTA, colocalization with TH (blue). Scale bar, 100 μm.

(C) In vivo anesthetized recording of light-evoked spikes from TH::Cre mouse: ChR2 in VTA.

(D) Optical stimulation parameters for home-cage interaction. For excitation, 473 nm light was delivered in 30 Hz bursts (eight pulses, 5 ms each) every 5 s. For inhibition, continuous 591 nm light was delivered.

(E) Summary of light-evoked changes in social interaction after bidirectional control of DA neurons. Phasic stimulation of VTA cell bodies increased social interaction compared to eYFP (n = 17 ChR2 and n = 18 eYFP, LME model, $t_{57} = 2.31$, $p = 0.03$), whereas inhibition of VTA cell bodies decreased interaction (n = 10 eNpHR3.0 and n = 15 eYFP, LME model, $t_{57} = -2.09$, $p = 0.04$).

(F) Neither stimulation nor inhibition of VTA cell bodies significantly affected novel object interaction ($p > 0.05$).

Error bars represent SEM. See also Figure S2.

these otherwise rapidly habituating signals could increase the overall amount of social interaction. To test this hypothesis, we selectively expressed a channelrhodopsin in VTA-DA neurons by injecting a Cre-dependent AAV encoding ChR2 fused to eYFP (ChR2-eYFP) into VTA of TH::Cre mice (TH-ChR2, Figure 2A), an approach previously shown to target DA neurons in the same region of lateral VTA with >98% specificity (Tsai et al., 2009). TH-positive neurons showed robust ChR2 expression (Figure 2B) and reliable elicitation of action potentials using 5 ms pulses of 473 nm light (Figure 2C). To assess the contribution of these neurons to social behavior, we employed the home-cage social interaction assay (with novel object control) as for fiber photometry, in which test mice in the home cage were separately exposed to two different stranger mice, one of which was paired with optical stimulation of VTA (counterbalanced for order of stimulation). Stimulation was delivered in 30 Hz bursts of light (eight pulses, 5 ms each; Figure 2D) every 5 s throughout the assay, a phasic pattern shown to evoke high levels of DA release (Adamantidis et al., 2011; Tsai et al., 2009). We then compared total time spent in active investigation between light-off and light-on epochs; scoring was conducted blind to genotype.

Phasic stimulation significantly increased investigation of the novel mouse, with no effect on controls (Figure 2E; n = 17 ChR2, n = 18 eYFP, LME model, $t_{57} = 2.31$, $p = 0.03$; similar prosocial effects were also observed in male-male interactions, n = 12, $p = 0.02$, data not shown). To test whether VTA-DA cells were not only sufficient to increase social behavior, but also necessary for full expression of social behavior, we inhibited VTA-DA neurons using an enhanced halorhodopsin (eNpHR3.0) and found a significant decrease in social interaction (Figure 2E; n = 10 eNpHR3.0, n = 15 eYFP, LME model, $t_{57} = -2.09$, $p = 0.04$). These same conditions of VTA stimulation and inhibition had no effect on investigation of a novel object (Figure 2F, Wilcoxon signed-rank test, $p = 0.41$) or locomotion (Figure S2, Wilcoxon signed-rank test, $p = 0.85$). Together, these optogenetic data demonstrate that phasic activity of VTA-DA neurons is sufficient to drive social interaction and that inhibiting activity in this population impairs normal social behavior.

The observed selective influence of experimentally modulated VTA-DA activity on social (but not novel object) behavior contrasts with the apparent similarity of naturally occurring VTA-DA activity peak magnitudes during social and novel object interactions. Given similar VTA-DA activity peak magnitudes in the two behaviors, it could be that precise timing of delivered activity is relevant (without which the causal impact is not seen) or that naturally occurring VTA-DA activity peaks are present in but do not causally drive the novel object behavior.

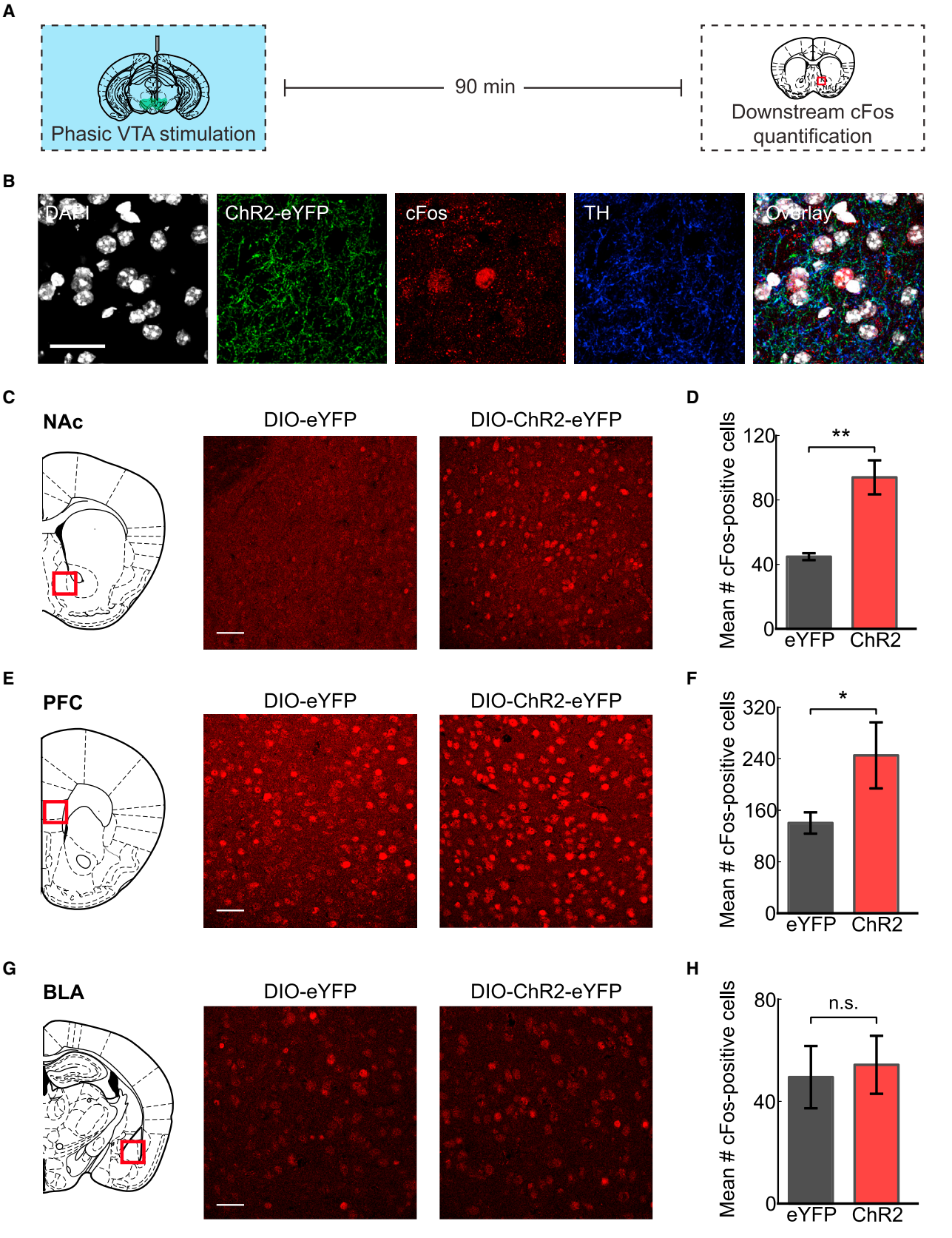

(legend on next page)

Indeed, the activity peaks may be only superficially similar in the two cases; a causally relevant subpopulation of VTA-DA neurons (not resolved by VTA photometry) could be driving social behavior. Even among cells that share the same physical location and genetic type, causally relevant subpopulations may be present that are differentially connected (e.g., Warden et al., 2012) in a way that is resolvable by projection targeting; we thus next sought to identify and probe not only causal sufficiency, but also native predictive activity, of candidate projection populations during freely moving behavior.

Activation of VTA-NAc, but Not VTA-mPFC, Projections Favors Social Behavior

To guide these efforts, we sought to systematically identify candidate downstream projection targets. We began with a brain-wide survey of VTA optogenetic stimulation-evoked induction of cFos, a marker of prolonged neural activity elevation (Figures 3A and 3B). We found upregulation of cFos in NAc (Figures 3C and 3D) and mPFC (Figures 3E and 3F), but not in basolateral amygdala (BLA; Figures 3G and 3H; n = 4 ChR2, n = 4 eYFP; t test: NAc, p = 0.00006; mPFC, p = 0.002; BLA, p = 0.82). With the resulting knowledge that NAc and mPFC were recruited by precisely the same optogenetic stimulation that increased social behavior (Figure 2), we next carried out optogenetic targeting of VTA cells projecting to each of these two regions in social interaction. We injected the same Cre-dependent ChR2 virus into VTA but targeted the optical fiber to either NAc or mPFC to activate VTA axons within these regions. Activation of cells with VTA-to-NAc projections (Figure 4A) sufficed to increase social interaction (Figure 4B, n = 11 ChR2, n = 12 eYFP, LME model, t_{30} = 7.11, p = 0.039) without affecting locomotion or novel object investigation (Figures S3A and S3B; Wilcoxon signed-rank test, p = 0.62 and p = 0.63, respectively). Activation of the VTA-mPFC projection (Figure 4C), on the other hand, had no effect on social interaction (Figure 4D; n = 7 ChR2, n = 7 eYFP, LME model, t_{12} = 0.11, p = 0.39). This mPFC projection might instead be relevant in part to behavioral responses of negative valence, as mPFC-projecting VTA DA neurons respond ex vivo to potentially aversion-related stimuli (Lammel et al., 2011). Indeed, we found that driving the VTA-mPFC projection was sufficient to account for anxiety-like effects of direct VTA stimulation (Figure S3C–S3F; n = 17 ChR2, n = 18 eYFP, p = 0.01 for cell bodies; n = 7 ChR2 and n = 7 eYFP, p = 0.02 for mPFC projection) and sufficed to cause conditioned place aversion (Figures S3G–S3I; n = 12 ChR2, n = 14 eYFP, Wilcoxon signed-rank test, p = 0.02), highlighting the functional specificity of distinct VTA projections.

Although the subpopulation of VTA neurons projecting to NAc sufficed to mediate prosocial effects of VTA stimulation, NAc-terminating VTA axons were not distinguished from possible axons passing through the NAc. To address this question, we injected Cre-dependent DIO-ChR2 AAV into the VTA of wild-type mice and injected AAV carrying a wheat germ agglutinin (WGA)-Cre recombinase fusion, which crosses trans-cellularly into local axon terminals and is transported to upstream somata (Dong et al., 2011; Yuan et al., 2011), into medial NAc (Figure 4E). With this approach (previously used to retrogradely target circuits; Gradinaru et al., 2010; Xu and Südhof, 2013), ChR2 is targeted to the subpopulation of VTA cells terminating in NAc. With fiber-optic placement directly above VTA (Figure 4F), we found that activation of cells with this connectivity sufficed to increase social interaction (Figure 4G; n = 14 ChR2, n = 11 eYFP, t_{23} = 2.53, p = 0.02) without affecting locomotion or novel object investigation (data not shown; Wilcoxon signed-rank test, p = 0.85 and p = 0.53, respectively). This approach gave sparse but strong expression of ChR2 in VTA and selective expression of ChR2 in fibers in NAc, but not mPFC or BLA (Figure 4H), supporting previous findings that VTA subpopulations projecting to these regions are nonoverlapping (Lammel et al., 2008) and indicating that behavioral effects are not attributable to antidromic spike propagation to collateral projections toward mPFC or BLA. Together, these results demonstrate that driving activity in VTA-NAc projections is sufficient to increase social interaction. Figure 4I summarizes behavioral effects of all VTA optogenetic interventions, illustrating the increasingly robust prosocial effect resulting from more projection-specific interventions.

Elevated NAc Activity in Prosocial Optogenetic Control and Native Social Behavior

We examined expression of these social behavior-related activity processes in NAc, using electrophysiology both in the anesthetized state and in freely moving animals during social interaction. First, during optogenetic stimulation in VTA of anesthetized animals, we observed increases in NAc firing (Figures 5A–5C): ~2-fold increased multiunit activity over several seconds following the VTA burst and an even larger increase close to the burst itself (Figures 5B and 5C; p < 0.001), consistent with timescales expected from DAergic neuromodulation.

We next investigated NAc activity during social behavior. Further supporting this link, we found that brief social interaction led to robust cFos induction in NAc (Figure 5D; p = 0.027). Next, we implanted TH-ChR2 animals with an optical fiber in VTA and a 16 electrode recording array in NAc; recording from awake animals alone in the home cage, we observed a consistent

Figure 3. Downstream Regions Recruited by Optogenetic VTA Stimulation

(A) Animals were stimulated for 5 min (home cage) and sacrificed 90 min later.

(B) Confocal images: ChR2-eYFP in VTA-originating fibers in NAc; induction of NAc cFos by VTA stimulation. (White) DAPI nuclear stain; (green) ChR2-eYFP; (red) cFos; (blue) anti-TH labeling of DA fibers. Scale bar, 25 μm.

(C) Images of NAc medial shell from eYFP and ChR2 slices; increased cFos+ NAc cells in ChR2 brain following VTA stimulation.

(D) cFos induction by VTA stimulation: NAc cFos increase in ChR2 compared to control (n = 4 eYFP, n = 4 ChR2; t test, p = 0.00006).

(E) Images of PFC from eYFP control and ChR2 slices; increased cFos+ PFC cells in the ChR2 brain following VTA stimulation.

(F) cFos induction by VTA stimulation: PFC cFos increase in ChR2 compared to control (n = 4 eYFP, n = 3 ChR2; t test, p = 0.002).

(G) Images of BLA from eYFP and ChR2 slices; no change in cFos+ PFC cells in the ChR2 brain following VTA stimulation.

(H) BLA cFos induction by VTA stimulation; no difference between ChR2 and control (n = 4 eYFP, n = 4 ChR2; t test, p = 0.82).

Error bars represent SEM.

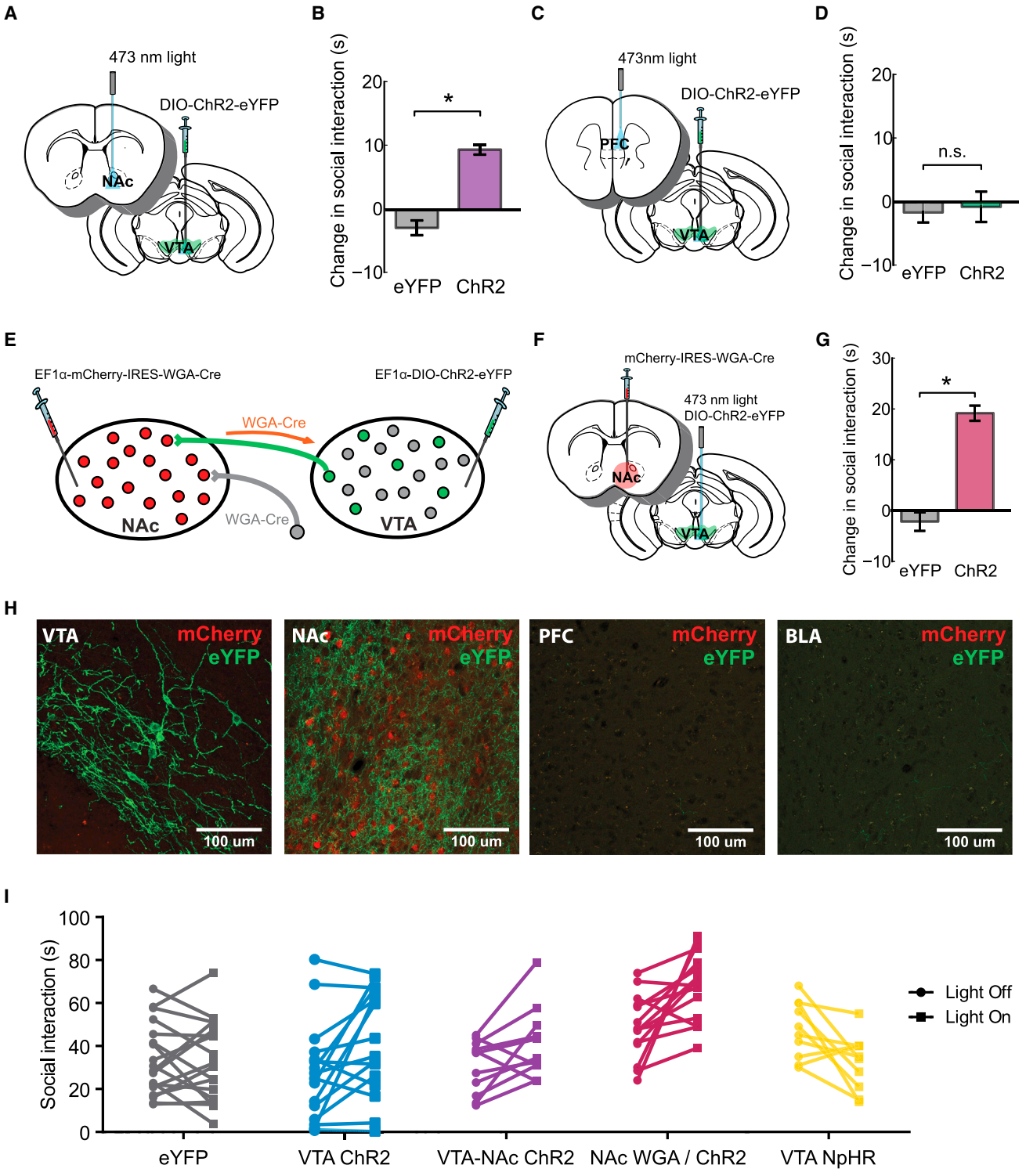

Figure 4. Projection-Specific VTA Control of Social Behavior

(A) ChR2 in VTA DA neurons and optical fiber implantation above NAc, targeting VTA-to-NAc projections.

(B) Phasic stimulation of VTA-originating axons in NAc increased social interaction in ChR2 animals (purple) compared to controls (gray) (n = 11 ChR2, n = 12 eYFP; LME model, $t_{30} = 7.11$, $p = 0.039$).

(C) ChR2 expression in VTA DA neurons and optical fiber implantation above PFC, targeting VTA-to-PFC projections.

(legend continued on next page)

light-evoked increase in NAc firing during optical drive of VTA-DA neurons comparable to that observed in anesthetized animals (Figure S4). To determine whether NAc cell firing naturally increased when animals engaged in social interaction, we recorded during exploration of an apparatus consisting of a chamber containing a stranger conspecific, and an otherwise identical neutral chamber (Figure 5E). This behavioral setting combined with video tracking allowed for temporally precise correlation of neural activity with defined social and neutral zones. We found that NAc multiunit activity was significantly higher when the test mouse was exploring the social chamber compared to the neutral chamber (Figures 5F and 5G; $p = 0.025$). Consistent with this increase in NAc firing during social behavior, bidirectional optogenetic modulation of VTA-NAc circuit elements (which modulated NAc firing in anesthetized and awake animals) produced the same bidirectional effects on social behavior in the three-chamber apparatus as in the home-cage social assay (Figure S4).

Detection of Native VTA-NAc Activity in Social, but Not Novel Object, Interaction

Though these data were consistent with the hypothesized importance of the VTA-NAc projection in social behavior, direct observation of endogeneous activity in the projection during social behavior remained lacking. Though achievable in superficial or transparent preparations (Dreosti et al., 2009; Petreanu et al., 2012), here (and in general), this would require measuring a previously inaccessible but fundamental neural circuit quantity: native activity in a specific deep projection during behavior. Fiber photometry (Figure 1) was designed for this technical challenge, and we next tested real-time tracking of Ca^{2+} transients in genetically specified VTA inputs to NAc. Using TH-GCaMP mice, we implanted an optical fiber in medial NAc to detect activity specifically in axon fibers corresponding to the projection in question (Figure 6A) during home-cage social interaction and novel object investigation (Figure 6B).

We observed robust GCaMP signals across many social interaction bouts, demonstrating that fiber photometry can be used to selectively record from neuronal projections (Figures 6B and 6C) during behavior. We observed smaller projection activation to novel object (Figures 6C and 6D and Movies S3 and S4; $n = 11$, Wilcoxon signed-rank test, mean peak dF/F: 6.9% ± 1.4% for social, 3.5% ± 0.7% for novel object, $p = 0.016$). Moreover, decay kinetics of social and novel peaks across bouts were different (fitting peak fluorescence to $Ae^{-kb} + c$ as before; novel object, $k = 0.0012$, $r^2 = 0.60$; social, $k = 0.2491$, $r^2 = 0.80$; Figure 6E), as were peak fluorescence distributions between social and novel object conditions (log-rank test: $p = 0.004$, $n = 208$ social; $n = 94$ object). Stronger encoding of social than of object interactions by the VTA-NAc projection (not seen at the cell bodies) supports the hypothesis that there are distinctly wired relevant subpopulations of VTA neurons. This conclusion was further supported by prediction and causal mediation analyses (as above for cell bodies). Peak Ca^{2+} activity during social interaction again predicted shorter latency to next interaction ($Z = -4.83$, $p < 0.0001$), whereas time since target introduction predicted longer latency ($Z = 5.80$, $p < 0.0001$), as expected and consistent with cell body findings. In contrast, the effect for cell bodies in novel object manipulation could not be found in projections to NAc (peak Ca^{2+} effect: $Z = 0.003$, $p = 0.99$; time-elapsed effect: $Z = 0.48$, $p = 0.64$). Causal mediation analysis found strong direct effects for the VTA-NAc projection in social interaction (Figure 6F; 68.2% average direct effect, 31.8% average indirect effect mediated by time elapsed; both $p < 0.0001$), similar to cell body results, with no significant direct or mediation effects for the novel object.

We sought to capitalize on this ability to track projection activity during behavior by probing in greater detail the encoding of specific behaviors by the VTA projection to NAc (in comparison with activity in VTA cell bodies) using multifactorial high-resolution quantitative behavioral assessment. We first employed an automated peak-finding algorithm (Experimental Procedures) to detect all Ca^{2+} peaks throughout the 5 min testing period, blind to mouse behaviors, for social and novel object conditions during both VTA cell body and VTA-NAc projection recordings. Next, we automatically segmented video clips centered (± 1 s) around the time of each Ca^{2+} peak and scored video segments for interaction, approach, withdrawal, ambulation, grooming, rest, burrowing, rearing, and head extension (Experimental Procedures). Based on results for Ca^{2+} peak size, decay profile, signal distribution, and causal mediation analyses above, we hypothesized that, for social behavior, the percentage of total Ca^{2+} peak activity representing target-relevant interaction behaviors would either remain the same or increase while recording from VTA-NAc projections compared to cell bodies (Figure 6) and would decrease for novel object behavior.

Stacked area plots of all VTA-DA Ca^{2+} peak times subdivided by behavioral category (Figures 7A and 7B) allowed direct comparison of total peak activity over time attributable to each category, including as a percent of total overall Ca^{2+} peak activity. In

(D) Phasic stimulation of VTA-originating axons in PFC had no effect on social interaction in ChR2 animals (blue) or controls (gray) ($n = 7$/group; LME model, $t_{12} = 0.11$, $p = 0.39$).

(E) Injection of mCherry-labeled WGA-Cre into NAc and Cre-dependent ChR2-eYFP into VTA of wild-type mice. WGA-Cre is trans-synaptically transported to all cells upstream of the NAc (orange arrow), but ChR2 expression is only activated in the subset of VTA neurons topologically defined by projections to medial NAc.

(F) ChR2 in the subset of VTA neurons that project to medial NAc; optical fiber implantation above VTA.

(G) Phasic stimulation of this subpopulation of VTA neurons increased social interaction in ChR2 animals (magenta), but not controls (gray) ($n = 14$/group; LME model, $t_{23} = 2.53$, $p = 0.02$).

(H) Sparse but strong ChR2-eYFP expression in VTA using this dual-virus system. ChR2-eYFP labels VTA fibers in medial NAc, where WGA-Cre virus was injected, with negligible labeling of PFC or BLA fibers. Scale bars, 100 μm.

(I) Summary of bidirectional effects of VTA interventions in individual animals. Consistency of prosocial effects increased with ChR2 projection specificity, and optical inhibition of VTA decreased social interaction. (Gray) eYFP controls; (blue) VTA DA cell body stimulation; (purple) VTA-NAc axonal stimulation; (magenta) WGA-Cre-isolated VTA-NAc projection; (yellow) VTA DA cell body inhibition with eNpHR3.0.

Error bars represent SEM. See also Figure S3.

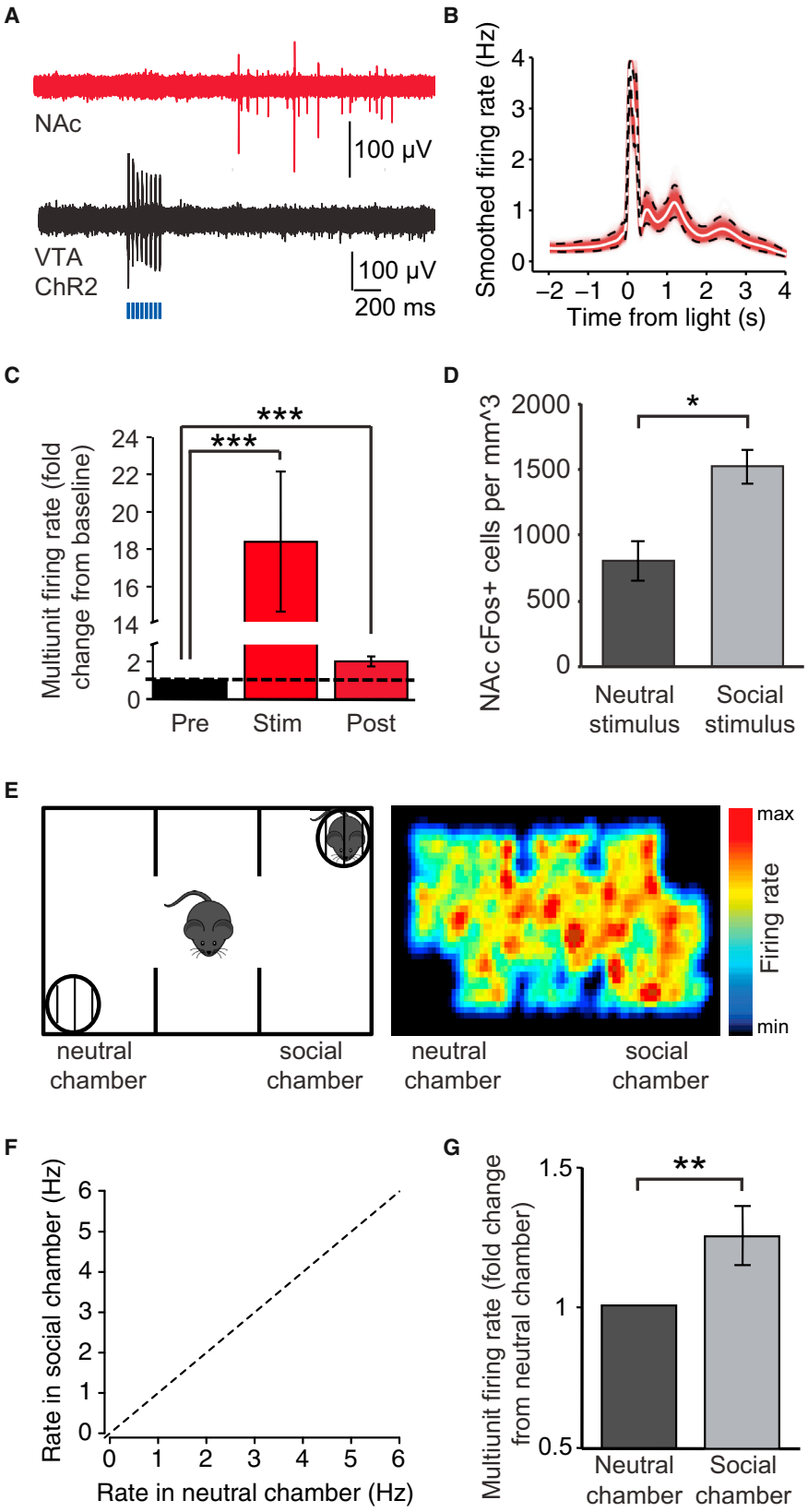

Figure 5. Electrophysiologic Assessment in NAc of Increased Social Behavior

(A) NAc activity (red) evoked by VTA stimulation (black).

(B) PSTH: light-evoked increase in NAc firing with one burst of VTA stimulation.

(C) Summary graph from (B): increase in NAc firing during/following a burst of light to VTA (Wilcoxon signed-rank test, $p < 0.001$).

(D) Increase in NAc cFos in unimplanted mice; social versus neutral stimulus (wire mesh cup) (5 min, n = 3/group; t test, $p = 0.03$).

(E) NAc activity in a freely moving animal exploring neutral and social environments. At right, heat-map shows the higher firing rate of NAc neurons in the social compared to the neutral chamber; warmer colors indicate higher firing rate.

(F) Correlation of firing rate in social versus neutral chamber for each multiunit recording site: note greater activity in social chamber; (black dots) individual multiunit recording sites; (dashed line) unity.

(G) NAc spiking is higher in a social environment (Wilcoxon signed-rank test, $p = 0.025$).

Error bars represent SEM. See also Figure S4.

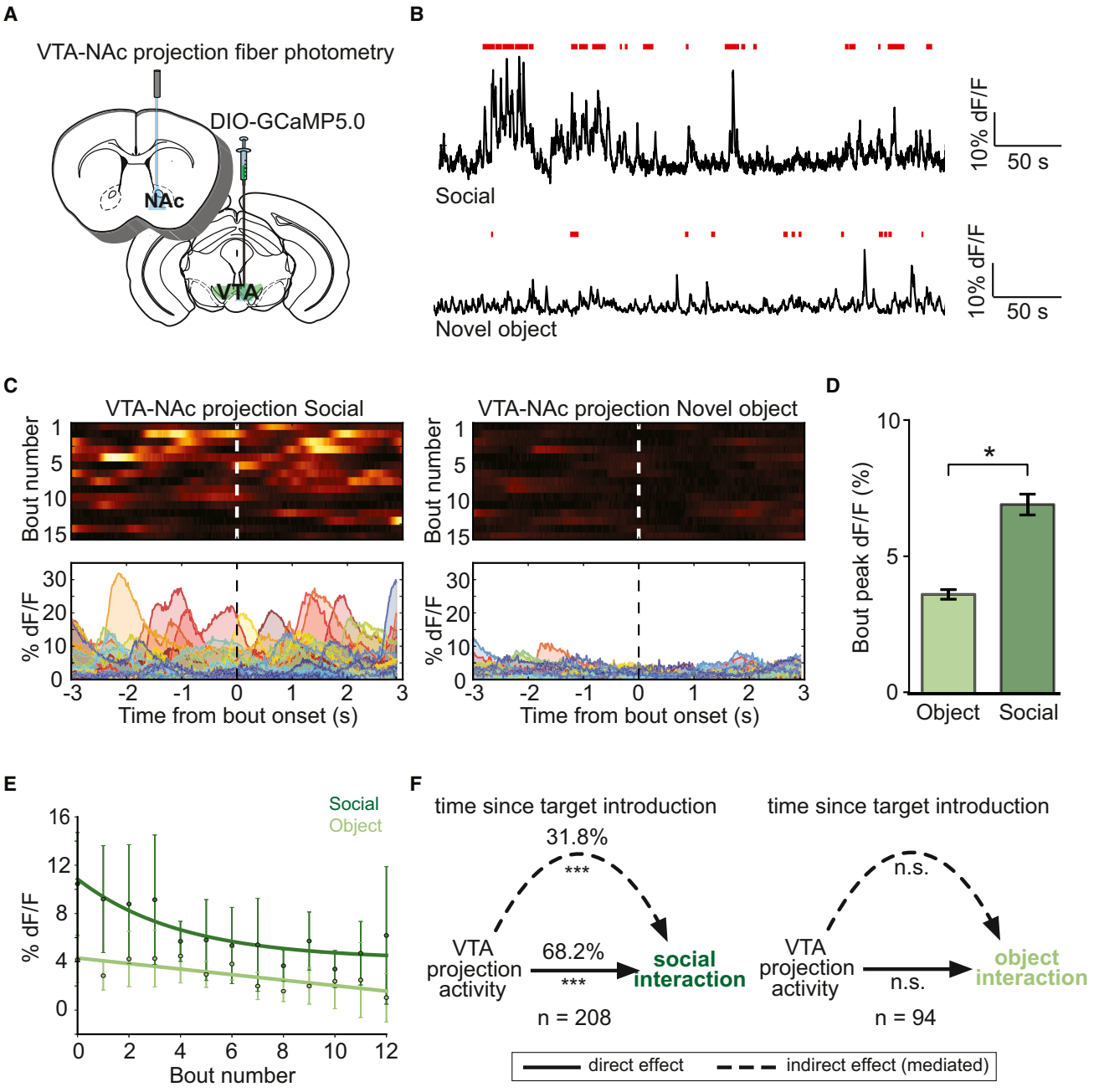

Figure 6. Fiber Photometry Assessment of DA Projection Activity in NAc during Social Interaction

(A) Fiber photometry of VTA projections in NAc.

(B) VTA projection activity during social (top) and novel object investigation (bottom; interaction bouts in red).

(C) Heatmaps (top) and peri-event plots (bottom) of NAc projection fluorescence aligned to start of interaction bout for social or novel object investigation. (Heatmaps) Warmer colors indicate higher fluorescence signal; (peri-event plots) warmer colors indicate earlier interaction bouts.

(D) NAc projections largely recapitulate social signals in VTA, with lower response to novel object (n = 11, Wilcoxon signed-rank test, mean peak fluorescence: 6.9% dF/F social, 3.6% dF/F novel object, $p = 0.016$).

(E) Decay of NAc projection signal across bouts. Decay in signal during social behavior is slower in projections than in cell bodies. Social decay rate = 0.2491, r^2 = 0.8; object decay rate = 0.0012, r^2 = 0.6.

(F) Directed graphical model of causal mediation analysis; though time elapsed partially mediated effects of VTA-NAc projection activity on latency to social interaction, the major effect was direct (68.2% average direct effect, 31.8% average indirect effect mediated by time elapsed; both $p < 0.0001$). No significant direct or indirect effects of VTA-NAc projection activity on latency to interact were observed in novel object investigation.

Error bars represent SEM.

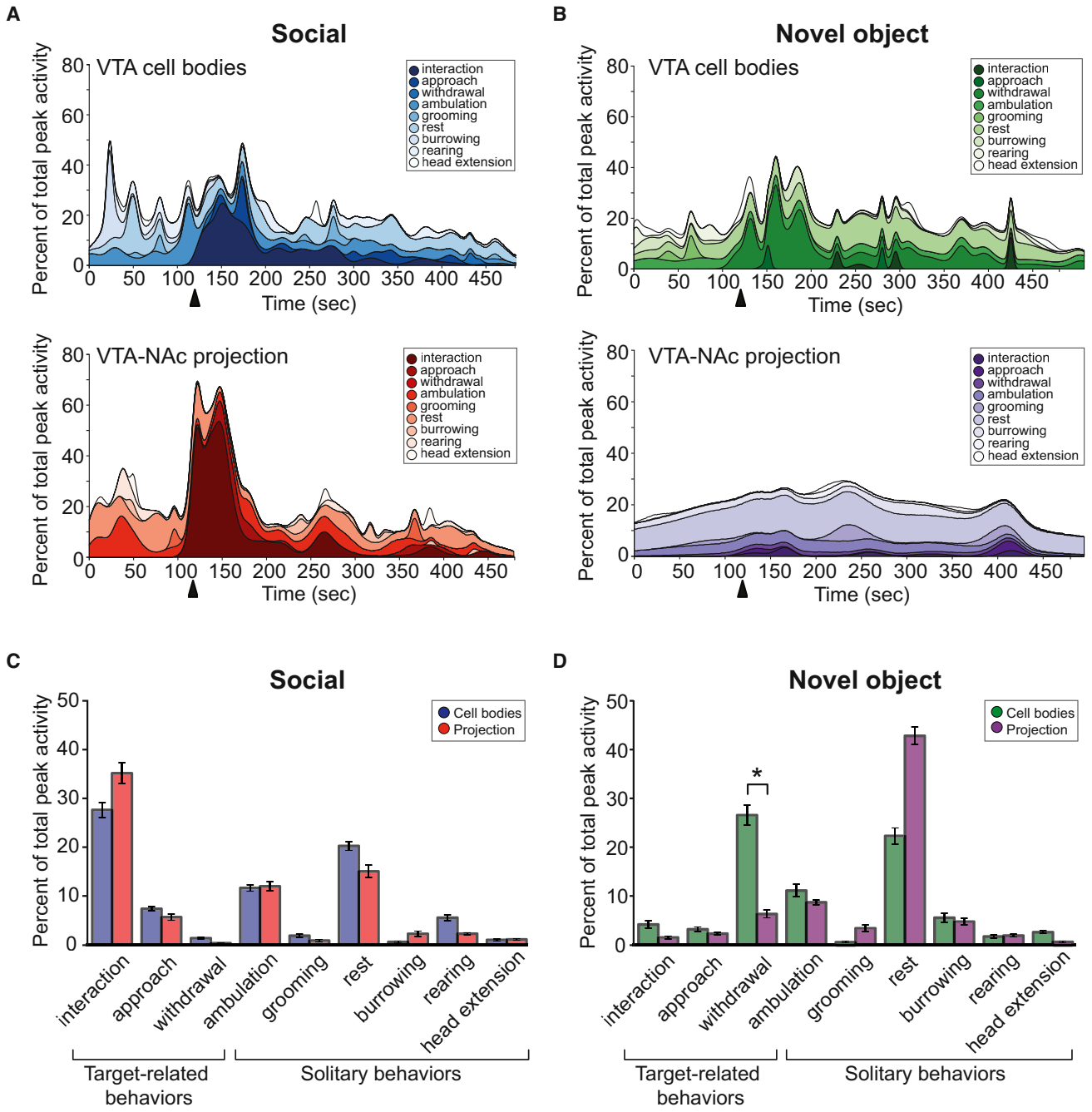

Figure 7. VTA-NAc Projection Activity Encodes Social Interaction

(A) Area plots, smoothed behavioral score: % total Ca^{2+} peaks representing specific social target-related and solitary behaviors during VTA cell body (top) and VTA-NAc projection (bottom) fiber photometry (n = 10 and n = 11 mice, respectively). (Arrows) Target introduction.

(B) Area plots, smoothed behavioral score: % total Ca^{2+} peaks representing specific novel-object-related and solitary behaviors during VTA cell body (top) and VTA-NAc projection (bottom) fiber photometry (n = 10 and n = 11 mice, respectively).

(C) Summary of data from (A): average % total Ca^{2+} peaks in target-related and solitary behaviors while recording VTA cell bodies (blue) and VTA-NAc projections (red) in the social assay. Note the encoding of social interaction by VTA cell body and VTA-NAc projection activity.

(D) Summary of data from (B): average % total Ca^{2+} peaks in target-related and solitary behaviors while recording VTA cell bodies (green) and VTA-NAc projections (purple) in the novel object assay. After correcting for multiple comparisons, only VTA-NAc projection activity at withdrawal represented a significantly smaller proportion of total peak activity compared to VTA cell body activity (two-sample permutation t test; p = 0.034 [Holm-corrected], n = 11), suggesting a specific reduction of object-related activity in VTA-NAc projections (the largest contributor to activity peaks in the novel object VTA cell body assay).

Error bars represent SEM.

the social case, a larger proportion of total Ca^{2+} peak activity occurred during interaction for VTA-to-NAc projections than for cell bodies, further supporting the conclusion that this projection more selectively encodes social interaction than does the cell body signal (Figure 7A). For novel object behavior, both cell bodies and projections poorly encoded approach or interaction (Figure 7B); interestingly, whereas the VTA cell bodies seemed to strongly encode withdrawal from the object (as in Figure 1H), the VTA-NAc projection only weakly encoded this specific behavior (Figure 7B). Across the entire 5 min testing period, VTA-NAc projections showed a decreased proportion of Ca^{2+} peak activity (compared with VTA cell body data) occurring during target-relevant behavior (accounted for by withdrawal) in the case of novel object, but not social, behavior (Figures 7C and 7D). These data together support the conclusion that VTA-NAc projection activity represents a signal with specific importance to social behavior relative to object interactions.

Necessity and Sufficiency of NAc D1R Activity for Social Behavior Modulation

To assess the final mechanistic step in this projection, we tested social-modulatory effects of postsynaptic cells and receptors in NAc. Most NAc cells are medium spiny neurons (MSNs), which can be divided into two broad categories defined by the type of DA receptor expressed (D1R or D2R, which couple to G_s- and G_i- signaling pathways, respectively [Beaulieu and Gainetdinov, 2011], with different roles in modulating reward [Lobo and Nestler, 2011]). To determine which DA receptor could be involved in mediating effects of VTA stimulation, we infused D1- or D2-specific antagonists (SCH23390 and raclopride, respectively) into the NAc prior to optical stimulation in social interaction (Figure 8A). Infusion of D1R, but not D2R, antagonist into NAc attenuated the prosocial effect of light, but not baseline levels of interaction (Figures 8B and S5; n = 15, LME model, t_{18} = 2.29, p = 0.035), indicating that DA signaling through D1Rs in NAc is necessary for mediating the social behavior increase elicited by VTA-DA neuron stimulation.

To test the sufficiency of D1R-expressing MSNs in social behavior with temporal precision, we sought to develop an engineered D1R that could be acutely controlled with light in behaving animals. We employed the OptoXR approach (Airan et al., 2009) to engineer direct optical control of D1R-mediated G_s signaling by replacing the intracellular loops of rhodopsin with those of D1R to form a chimeric Opto-D1 (Figures 8C and S5). In HEK cells expressing the Opto-D1-eYFP fusion construct, selective upregulation of cAMP (G_s), but not IP3 (G_q) or cGMP (G_t), signaling pathways was driven by light, as anticipated (Figure 8D, n = 3, four readings each, unpaired t test, p = 0.002).

To fully leverage the specificity of sufficiency testing with Opto-D1, it would be ideal to transduce only cells that normally express D1R. We therefore next injected a Cre-dependent AAV virus carrying Opto-D1 into the NAc of Drd1::Cre transgenic mice to restrict expression to D1R MSNs (Figure 8E). Light (473 nm) under these conditions was sufficient to increase social interaction (Figure 8F, n = 10 Opto-D1, n = 10 eYFP, LME model, t_{18} = 2.64, p = 0.018) without affecting locomotion or novel object investigation (Figure S5; Wilcoxon signed-rank test, p = 0.52, 0.40, respectively). Optrode recordings of Opto-D1 effects in NAc revealed ~3-fold light-increased multiunit activity (Figures 8G–8I; Wilcoxon signed-rank test, p = 0.01). Interestingly, the magnitude and direction of this D1R-mediated change in NAc spiking was consistent with the increase in NAc activity observed during natural social interaction as well as optogenetic VTA activation (Figure 5). However, these data do not demonstrate that such an increase in spiking could suffice to drive increased social behavior; indeed, D1R signaling could also affect many distinct aspects of cellular physiology and biochemistry. Therefore, as a final test of whether evoked increases in activity of NAc D1 cells could suffice to drive social interaction, we injected DIO-ChR2 AAV into the NAc of Drd::Cre mice (Figure 8J). Direct stimulation of firing in NAc D1 cells was indeed sufficient to produce a significant increase in social interaction compared to controls (Figure 8K, n = 6, LME model, t_{11} = 2.26, p = 0.039).

DISCUSSION

Here, we have developed and applied fiber photometry for direct measurement of a previously inaccessible variable in neuroscience: the activity of specified neuronal afferents projecting to a particular deep downstream target during mammalian behavior. Using this method, we have found that an increase in activity in VTA DA neurons, especially in their projections to the NAc, predicts social interaction in freely behaving mice. Fiber photometry can be used together with optogenetics to determine both natural and causal dynamics in both cell bodies and projections underlying complex behavior.

This ability to directly measure activity of projections between brain regions provides a new source of data on dynamics of information flow (Deisseroth, 2014). In network modeling, groups of neurons with similar projection patterns can be modeled as nodes in a network and projections to downstream regions represented as directed links (Bullmore and Sporns, 2009). In simplified projection-based network dynamics terminology, each link from region i to a downstream region j can be modeled as providing a time-varying input $i \rightarrow j(t)$, which acting through a separate aggregate synaptic strength parameter $w_{ij}(t)$, defines the net influence of that projection from the neurons in region i onto those in region j at time t, contributing to the aggregate postsynaptic response $j(t)$. Fiber photometry of projections now allows for the first time deep observation of these time-varying inputs $i \rightarrow j(t)$ (independent of $w_{ij}(t)$ and $j(t)$) that represent the endogenous dynamics specific to one projection in the brain that can be thought of as the time-varying ''traffic'' over the targeted link $i \rightarrow j$. It is worth noting that, although the local field potential (LFP) can reflect synaptic input in a region (Lindén et al., 2011), spontaneous LFP signals represent aggregate local readouts that cannot provide information on a specific projection from one brain region to another; moreover, even evoked LFP signals, in which an upstream brain region is stimulated, cannot report the native activity of a specific projection during behavior; nor do such electrically evoked signals provide for specific recruitment of a genetically and topologically defined projection. To our knowledge, this fundamental network parameter $i \rightarrow j(t)$ has not been generally accessible and may define a key new measurement for dynamical network modeling.

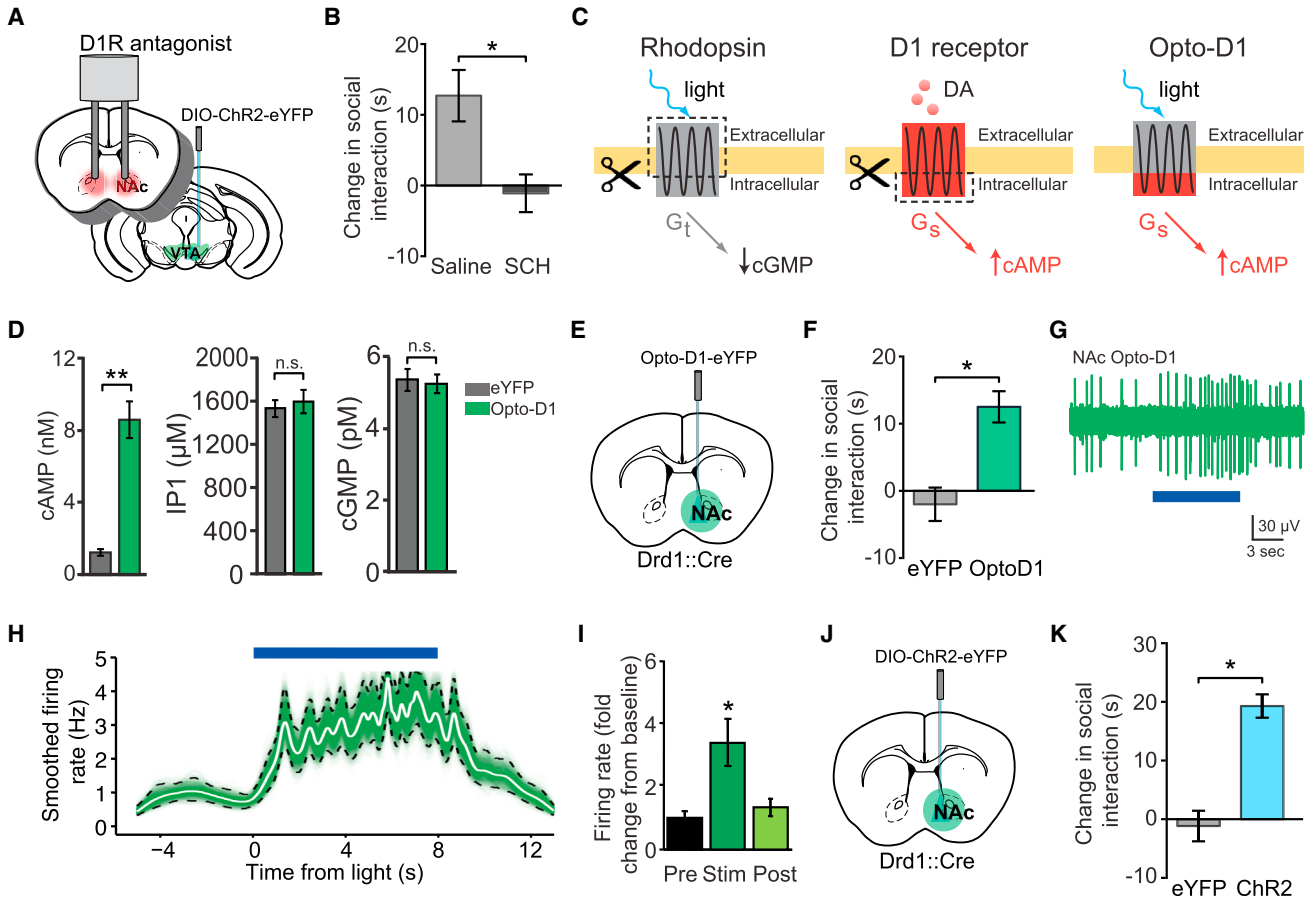

Figure 8. Postsynaptic NAc D1 Cells and Receptors in Natural and VTA Stimulation-Driven Social Behavior

(A) Infusion of D1 receptor (D1R) antagonist SCH23390 into the NAc prior to VTA stimulation during social interaction.

(B) Compared to control saline infusion, D1R antagonism attenuated light-evoked increases in social behavior (n = 15, LME model, $t_{18} = 2.29$, $p = 0.035$).

(C) Opto-D1 design: replacing intracellular loops of rhodopsin with those of D1R.

(D) In vitro GPCR signaling assays show selective upregulation of cAMP, but not IP3 or cGMP pathways by Opto-D1 (n = 3 samples, four readings each, unpaired t test, $p = 0.002$).

(E) Infusion of DIO-Opto-D1 virus into the NAc of Drd1::Cre mice for selective expression in D1R+ NAc cells.

(F) Illumination of Opto-D1 in NAc D1 cells with continuous 473 nm light increased social interaction compared to eYFP controls (n = 10 per group, LME model, $t_{18} = 2.64$, $p = 0.018$).

(G) Example recording of NAc activity with Opto-D1 activation.

(H) PSTH: light-evoked increase in NAc firing with Opto-D1.

(I) Summary graph from (H): increase in NAc firing during activation of Opto-D1 (Wilcoxon signed-rank test, $p = 0.01$).

(J) Infusion of DIO-ChR2 into NAc of Drd1::Cre mice.

(K) Tonic 10 Hz stimulation of NAc D1R cells increased social interaction (n = 6, LME model, $t_{11} = 2.26$, $p = 0.039$).

See also Figure S5.

Indeed, this kind of parameter appears especially predictive in behavior (Figure 6). Moreover, projection-specific activity is also particularly important for causal elicitation of complex behaviors, as found here and elsewhere (reviewed in Deisseroth, 2014). Optogenetic enhancement of phasic activity in VTA-DA somata increased social behavior (concordant with the fiber photometry data and confirming that these neurons are causally involved in driving social interaction), but it is the projections to NAc and not other downstream regions such as PFC that predict and mediate this effect. Projection-specific optogenetic manipulations complement specificity of fiber photometry by enabling control of the corresponding dynamics $i \rightarrow j(t)$. Along with development and application of Opto-D1R, enabling causal identification of postsynaptic NAc D1 MSNs regulating social behavior, these results demonstrate integrative value of complementary optical techniques in causally mapping specific projections and postsynaptic targets within neural circuitry.

Our observation that VTA DA neuron activity is causally involved in bidirectional modulation of same-sex social interaction supports prior pharmacological studies implicating DA in affiliative behaviors (Aragona et al., 2006; Curtis and Wang, 2005; Gingrich et al., 2000; Liu and Wang, 2003), though it had been previously difficult to determine the precise site and mechanism of action of DA as receptors are expressed

postsynaptically as well as presynaptically on VTA terminals (Benoit-Marand et al., 2001; Palij et al., 1990), and pharmacological agents could exert behavioral effects either by enhancing DA signaling downstream or by dampening VTA activity via inhibitory autoreceptors. Additionally, NAc-projecting VTA neurons may co-release other neurotransmitters such as glutamate (Stuber et al., 2010), and DA pharmacological manipulations do not typically capture this synergy present in endogenous VTA activity. The findings presented here illuminate not the role of a specific neurotransmitter but, rather, the circuit elements and dynamics in modulation of social behavior, defining relevant projections as well as pre- and postsynaptic cell types in mesolimbic circuitry.

An increase in NAc spiking occurred when animals chose to explore the social target, and two distinct prosocial optogenetic manipulations (VTA ChR2 and NAc Opto-D1 stimulation) at different steps in the putative circuit each increased NAc multiunit activity. These results are consistent with in vivo recordings showing increased NAc activity associated with reward-related behaviors, as well as studies implicating D1Rs in enhancing activity of MSNs (Lobo and Nestler, 2011; Moratalla et al., 1996). While the effects of DA on excitability are complex and depend on glutamatergic tone in NAc, activation of D1Rs is generally associated with increasing excitability of MSNs and activation of D2Rs is thought to decrease MSN excitability (Lobo and Nestler, 2011; Perez et al., 2006; Podda et al., 2010). Our results are also concordant with previous reports implicating D1 MSNs in enhancing the effects of rewarding stimuli (Lobo and Nestler, 2011). Mice display appetitive responses to same-sex social interaction even before reaching sexual maturity (Panksepp et al., 2007; Panksepp and Lahvis, 2007), and it may be that this natural reward can be provided or reinforced just as stimulating D1 MSNs drives animals to seek conditioned reward (Lobo et al., 2010).

Here, we have taken steps toward facilitating circuit-level understanding of the neural basis of complex behaviors by addressing the roles of specific pre- and postsynaptic cell types defined by genetic and projection profile and by providing a deep window into a fundamental network property (the direct real-time input from one brain region into another during mammalian behavior) with fiber photometry. In defining multiple components along an extended circuit regulating social behavior, we have explored the significance of specific cells, projections, and targets, rather than individual neurotransmitters. This approach may suggest circuit-based targets for further research into impaired social interaction and other neuropsychiatric disease-related symptoms and may be generally applicable for investigation of specific circuit elements in mammalian behavior.

EXPERIMENTAL PROCEDURES

Animals

Adult female mice (aged 8 weeks at the start of experimental procedures) were used for all behavioral experiments. Mice were housed on a reverse 12 hr light/dark cycle and were given food and water ad libitum. All animals were group housed except those implanted with chronic bundle electrodes. Estrous cycle stage was not examined as a factor in these studies. All experimental protocols were approved by the Stanford University IACUC following the National Institutes of Health guidelines for the Care and Use of Laboratory Animals.

Viral Constructs

To achieve cell-type-specific opsin expression in Cre driver lines, we cloned the GCaMP5g, ChR2(H134R), eNpHR3.0, and Opto-D1 genes into the double-floxed inverted open reading frame plasmid pAAV-EF1α-DIO-ChR2-YFP-WPRE (Sohal et al., 2009). The WGA-Cre construct was expressed in the plasmid pAAV-EF1α-mCherry-IRES-WGA-Cre.

Behavioral Testing

All tests were performed during the dark phase, and animals were acclimated to the behavior room for at least 1 hr before testing. A 3 m long fiber-optic patch-cord (Doric Lenses) was connected to the chronically implanted optical fiber with a zirconia sheath and was suspended above the behavioral testing environment to allow animals to move freely during stimulation. The patch-cord was connected to a 473 nm solid-state laser diode (OEM Laser Systems) with an FC/PC adaptor. A Master-8 pulse stimulator (A.M.P.I.) controlled laser output. Phasic stimulation of VTA cell bodies and axon terminals consisted of 30 Hz bursts of eight 5 ms pulses of 473 nm light delivered every 5 s at a light power output of 10 mW from the tip of the optical fiber. Activating light pulses for Opto-D1 consisted of continuous 473 nm light at 5 mW and 591 nm continuous light at 1 mW for eNpHR3.0. For detailed descriptions of behavioral assays, refer to the Experimental Procedures.

Fiber Photometry

The fiber photometry system used a 473 nm diode laser (Omicron Luxx) that was chopped at 400 Hz, reflected off a dichroic (Semrock, FF495), and coupled into a 600 μm 0.48 NA optical fiber (Thorlabs BFH48-600, important for minimal autofluorescence and signal recovery) using a 40× 0.65 NA microscope objective (Olympus) and fiber launch (Thorlabs), with the patchcord linked to an implanted 400 μm optical fiber with zirconia sheath. The laser intensity at the interface between the fiber tip and the animal ranged from 1.8–1.9 mW (but was constant across trials that were compared side by side). GCaMP fluorescence collected by the objective and transmitted by the dichroic was focused through a bandpass filter (Semrock, FF01-520/35) onto a NewFocus 2151 femtowatt silicon photoreceiver (Newport, DC Low mode), the output of which was directed through a lock-in amplifier (SR810 DSP, Stanford Research Systems, 3 ms time constant), digitized using a LabJack DAQ, and recorded by custom Python software. Signals were collected at a sampling frequency of 250 Hz.

Statistical Analysis

For behavioral experiments, all binary comparisons were tested using nonparametric Wilcoxon rank-sum tests (paired or unpaired as appropriate), and hypotheses involving more than two group means were tested using linear contrasts in a linear mixed effects (LME) model. Electrophysiological data were fit by block bootstrapping 1,000 times, applying a scaled adaptive nonparametric smoother ("akj" in R package "quantreg") to each of the bootstrap replicates and allowing the calculation of 95% confidence intervals for the mean firing rate over time while adaptively allowing for sharp changes in firing rate. Kaplan-Meier estimates were used to compare latency to interact for the social and novel object interaction behavior. For regressions of the latency to engage in social and novel object interactions onto peak Ca^{2+} recording values, we used survival regression ("survreg" in R's "survival" library). Causal mediation analyses were carried out using the "mediation" library in R. For a more detailed description of these tests, see the Experimental Procedures.

SUPPLEMENTAL INFORMATION

Supplemental Information includes Extended Experimental Procedures, five figures, and four movies and can be found with this article online at http://dx.doi.org/10.1016/j.cell.2014.05.017.

AUTHOR CONTRIBUTIONS

L.A.G. and K.D. designed all of the experiments and wrote the paper, and K.D. supervised all aspects of the work. L.A.G. conducted experiments and

analyzed data for all sections of the paper. L.G. and I.V.K. built the fiber photometry recording system and wrote custom software for fiber photometry data analysis. J.C.F. conducted behavioral experiments, histology, and in vivo optrode recordings.

ACKNOWLEDGMENTS

We thank the entire Deisseroth lab for helpful discussions and T. Jardetzky for use of a Biotek Synergy4 plate reader. L.A.G. is supported by a Stanford Bio-X Fellowship. L.G. is supported by NSF 0801700. L.E.F. is supported by the Stanford Medical Scientist Training Program. K.D. is supported by the Simons Foundation Autism Research Initiative, a Conte Center grant from NIMH, and NIDA, DARPA, the Gatsby Charitable Foundation, James Doty and the CCARE center at Stanford, the Stanford Institute for Neuroinnovation and Translational Neurosciences, and the Wiegers Family Fund. R.C.M. and S.L. were supported by a grant from the Simons Foundation Autism Research Initiative and a Conte Center grant from NIMH. All optogenetic tools and methods described are distributed and supported freely (http://www.optogenetics.org).

Received: February 12, 2014
Revised: April 30, 2014
Accepted: May 12, 2014
Published: June 19, 2014

REFERENCES

Adamantidis, A.R., Tsai, H.C., Boutrel, B., Zhang, F., Stuber, G.D., Budygin, E.A., Touriño, C., Bonci, A., Deisseroth, K., and de Lecea, L. (2011). Optogenetic interrogation of dopaminergic modulation of the multiple phases of reward-seeking behavior. J. Neurosci. *31*, 10829–10835.

Airan, R.D., Thompson, K.R., Fenno, L.E., Bernstein, H., and Deisseroth, K. (2009). Temporally precise in vivo control of intracellular signalling. Nature *458*, 1025–1029.

Akerboom, J., Chen, T.W., Wardill, T.J., Tian, L., Marvin, J.S., Mutlu, S., Calderón, N.C., Esposti, F., Borghuis, B.G., Sun, X.R., et al. (2012). Optimization of a GCaMP calcium indicator for neural activity imaging. J. Neurosci. *32*, 13819–13840.

Aragona, B.J., Liu, Y., Yu, Y.J., Curtis, J.T., Detwiler, J.M., Insel, T.R., and Wang, Z. (2006). Nucleus accumbens dopamine differentially mediates the formation and maintenance of monogamous pair bonds. Nat. Neurosci. *9*, 133–139.

Aravanis, A.M., Wang, L.P., Zhang, F., Meltzer, L.A., Mogri, M.Z., Schneider, M.B., and Deisseroth, K. (2007). An optical neural interface: in vivo control of rodent motor cortex with integrated fiberoptic and optogenetic technology. J. Neural Eng. *4*, S143–S156.

Beaulieu, J.M., and Gainetdinov, R.R. (2011). The physiology, signaling, and pharmacology of dopamine receptors. Pharmacol. Rev. *63*, 182–217.

Benoit-Marand, M., Borrelli, E., and Gonon, F. (2001). Inhibition of dopamine release via presynaptic D2 receptors: time course and functional characteristics in vivo. J. Neurosci. *21*, 9134–9141.

Brischoux, F., Chakraborty, S., Brierley, D.I., and Ungless, M.A. (2009). Phasic excitation of dopamine neurons in ventral VTA by noxious stimuli. Proc. Natl. Acad. Sci. USA *106*, 4894–4899.

Budygin, E.A., Park, J., Bass, C.E., Grinevich, V.P., Bonin, K.D., and Wightman, R.M. (2012). Aversive stimulus differentially triggers subsecond dopamine release in reward regions. Neuroscience *201*, 331–337.

Bullmore, E., and Sporns, O. (2009). Complex brain networks: graph theoretical analysis of structural and functional systems. Nat. Rev. Neurosci. *10*, 186–198.

Chaudhury, D., Walsh, J.J., Friedman, A.K., Juarez, B., Ku, S.M., Koo, J.W., Ferguson, D., Tsai, H.C., Pomeranz, L., Christoffel, D.J., et al. (2013). Rapid regulation of depression-related behaviours by control of midbrain dopamine neurons. Nature *493*, 532–536.

Chen, T.W., Wardill, T.J., Sun, Y., Pulver, S.R., Renninger, S.L., Baohan, A., Schreiter, E.R., Kerr, R.A., Orger, M.B., Jayaraman, V., et al. (2013). Ultrasensitive fluorescent proteins for imaging neuronal activity. Nature *499*, 295–300.

Cui, G., Jun, S.B., Jin, X., Pham, M.D., Vogel, S.S., Lovinger, D.M., and Costa, R.M. (2013). Concurrent activation of striatal direct and indirect pathways during action initiation. Nature *494*, 238–242.

Curtis, J.T., and Wang, Z. (2005). Ventral tegmental area involvement in pair bonding in male prairie voles. Physiol. Behav. *86*, 338–346.

Deisseroth, K. (2014). Circuit dynamics of adaptive and maladaptive behaviour. Nature *505*, 309–317.

Dong, Y., Li, J., Zhang, F., and Li, Y. (2011). Nociceptive afferents to the premotor neurons that send axons simultaneously to the facial and hypoglossal motoneurons by means of axon collaterals. PLoS ONE *6*, e25615.

Dreosti, E., Odermatt, B., Dorostkar, M.M., and Lagnado, L. (2009). A genetically-encoded reporter of synaptic activity in vivo. Nat. Methods *6*, 883–889.

Gingrich, B., Liu, Y., Cascio, C., Wang, Z., and Insel, T.R. (2000). Dopamine D2 receptors in the nucleus accumbens are important for social attachment in female prairie voles (Microtus ochrogaster). Behav. Neurosci. *114*, 173–183.

Gradinaru, V., Zhang, F., Ramakrishnan, C., Mattis, J., Prakash, R., Diester, I., Goshen, I., Thompson, K.R., and Deisseroth, K. (2010). Molecular and cellular approaches for diversifying and extending optogenetics. Cell *141*, 154–165.

Gradinaru, V., Thompson, K.R., Zhang, F., Mogri, M., Kay, K., Schneider, M.B., and Deisseroth, K. (2007). J. Neurosci. 27, 14231–1438.

Imai, K., Keele, L., and Tingley, D. (2010). A general approach to causal mediation analysis. Psychol. Methods *15*, 309–334.

Kalivas, P.W., and Nakamura, M. (1999). Neural systems for behavioral activation and reward. Curr. Opin. Neurobiol. *9*, 223–227.

Lammel, S., Hetzel, A., Häckel, O., Jones, I., Liss, B., and Roeper, J. (2008). Unique properties of mesoprefrontal neurons within a dual mesocorticolimbic dopamine system. Neuron *57*, 760–773.

Lammel, S., Ion, D.I., Roeper, J., and Malenka, R.C. (2011). Projection-specific modulation of dopamine neuron synapses by aversive and rewarding stimuli. Neuron *70*, 855–862.

Lammel, S., Lim, B.K., Ran, C., Huang, K.W., Betley, M.J., Tye, K.M., Deisseroth, K., and Malenka, R.C. (2012). Input-specific control of reward and aversion in the ventral tegmental area. Nature *491*, 212–217.

Leypold, B.G., Yu, C.R., Leinders-Zufall, T., Kim, M.M., Zufall, F., and Axel, R. (2002). Altered sexual and social behaviors in trp2 mutant mice. Proc. Natl. Acad. Sci. USA *99*, 6376–6381.

Lindén, H., Tetzlaff, T., Potjans, T.C., Pettersen, K.H., Grün, S., Diesmann, M., and Einevoll, G.T. (2011). Modeling the spatial reach of the LFP. Neuron *72*, 859–872.

Liu, Y., and Wang, Z.X. (2003). Nucleus accumbens oxytocin and dopamine interact to regulate pair bond formation in female prairie voles. Neuroscience *121*, 537–544.

Lobo, M.K., and Nestler, E.J. (2011). The striatal balancing act in drug addiction: distinct roles of direct and indirect pathway medium spiny neurons. Front. Neuroanat. *5*, 41.

Lobo, M.K., Covington, H.E., 3rd, Chaudhury, D., Friedman, A.K., Sun, H., Damez-Werno, D., Dietz, D.M., Zaman, S., Koo, J.W., Kennedy, P.J., et al. (2010). Cell type-specific loss of BDNF signaling mimics optogenetic control of cocaine reward. Science *330*, 385–390.

Lutcke, H., Murayama, M., Hahn, T., Margolis, D.J., Astori, S., Zum Alten Borgloh, S.M., Gobel, W., Yang, Y., Tang, W., Kugler, S., et al. (2010). Optical recording of neuronal activity with a genetically-encoded calcium indicator in anesthetized and freely moving mice. Front. Neural Circuits *4*, 9.

Mirenowicz, J., and Schultz, W. (1996). Preferential activation of midbrain dopamine neurons by appetitive rather than aversive stimuli. Nature *379*, 449–451.

Moratalla, R., Xu, M., Tonegawa, S., and Graybiel, A.M. (1996). Cellular responses to psychomotor stimulant and neuroleptic drugs are abnormal in

mice lacking the D1 dopamine receptor. Proc. Natl. Acad. Sci. USA *93*, 14928–14933.

Moy, S.S., Nadler, J.J., Perez, A., Barbaro, R.P., Johns, J.M., Magnuson, T.R., Piven, J., and Crawley, J.N. (2004). Sociability and preference for social novelty in five inbred strains: an approach to assess autistic-like behavior in mice. Genes Brain Behav. *3*, 287–302.

Palij, P., Bull, D.R., Sheehan, M.J., Millar, J., Stamford, J., Kruk, Z.L., and Humphrey, P.P. (1990). Presynaptic regulation of dopamine release in corpus striatum monitored in vitro in real time by fast cyclic voltammetry. Brain Res. *509*, 172–174.

Panksepp, J.B., and Lahvis, G.P. (2007). Social reward among juvenile mice. Genes Brain Behav. *6*, 661–671.

Panksepp, J.B., Jochman, K.A., Kim, J.U., Koy, J.J., Wilson, E.D., Chen, Q., Wilson, C.R., and Lahvis, G.P. (2007). Affiliative behavior, ultrasonic communication and social reward are influenced by genetic variation in adolescent mice. PLoS ONE *2*, e351.

Perez, M.F., White, F.J., and Hu, X.T. (2006). Dopamine D(2) receptor modulation of K(+) channel activity regulates excitability of nucleus accumbens neurons at different membrane potentials. J. Neurophysiol. *96*, 2217–2228.

Petreanu, L., Gutnisky, D.A., Huber, D., Xu, N., O'Connor, D.H., Tian, L., Looger, L., and Svoboda, K. (2012). Activity in motor-sensory projections reveals distributed coding in somatosensation. Nature *489*, 299–303.

Podda, M.V., Riccardi, E., D'Ascenzo, M., Azzena, G.B., and Grassi, C. (2010). Dopamine D1-like receptor activation depolarizes medium spiny neurons of the mouse nucleus accumbens by inhibiting inwardly rectifying K+ currents through a cAMP-dependent protein kinase A-independent mechanism. Neuroscience *167*, 678–690.

Puglisi-Allegra, S., and Cabib, S. (1997). Psychopharmacology of dopamine: the contribution of comparative studies in inbred strains of mice. Prog. Neurobiol. *51*, 637–661.

Robinson, D.L., Heien, M.L., and Wightman, R.M. (2002). Frequency of dopamine concentration transients increases in dorsal and ventral striatum of male rats during introduction of conspecifics. J. Neurosci. *22*, 10477–10486.

Robinson, D.L., Zitzman, D.L., Smith, K.J., and Spear, L.P. (2011). Fast dopamine release events in the nucleus accumbens of early adolescent rats. Neuroscience *176*, 296–307.

Schulz, K., Sydekum, E., Krueppel, R., Engelbrecht, C.J., Schlegel, F., Schröter, A., Rudin, M., and Helmchen, F. (2012). Simultaneous BOLD fMRI and fiber-optic calcium recording in rat neocortex. Nat. Methods *9*, 597–602.

Silva, A.J., and Ehninger, D. (2009). Adult reversal of cognitive phenotypes in neurodevelopmental disorders. J. Neurodev. Disord. *1*, 150–157.

Sohal, V.S., Zhang, F., Yizhar, O., and Deisseroth, K. (2009). Parvalbumin neurons and gamma rhythms enhance cortical circuit performance. Nature *459*, 698–702.

Stuber, G.D., Hnasko, T.S., Britt, J.P., Edwards, R.H., and Bonci, A. (2010). Dopaminergic terminals in the nucleus accumbens but not the dorsal striatum corelease glutamate. J. Neurosci. *30*, 8229–8233.

Tsai, H.C., Zhang, F., Adamantidis, A., Stuber, G.D., Bonci, A., de Lecea, L., and Deisseroth, K. (2009). Phasic firing in dopaminergic neurons is sufficient for behavioral conditioning. Science *324*, 1080–1084.

Tye, K.M., Mirzabekov, J.J., Warden, M.R., Ferenczi, E.A., Tsai, H.C., Finkelstein, J., Kim, S.Y., Adhikari, A., Thompson, K.R., Andalman, A.S., et al. (2013). Dopamine neurons modulate neural encoding and expression of depression-related behaviour. Nature *493*, 537–541.

Warden, M.R., Selimbeyoglu, A., Mirzabekov, J.J., Lo, M., Thompson, K.R., Kim, S.Y., Adhikari, A., Tye, K.M., Frank, L.M., and Deisseroth, K. (2012). A prefrontal cortex-brainstem neuronal projection that controls response to behavioural challenge. Nature *492*, 428–432.

Winslow, J.T. (2003). Mouse social recognition and preference. Curr. Protoc. Neurosci. *Chapter 8*, Unit 16.

Xu, W., and Südhof, T.C. (2013). A neural circuit for memory specificity and generalization. Science *339*, 1290–1295.

Young, L.J., and Wang, Z. (2004). The neurobiology of pair bonding. Nat. Neurosci. *7*, 1048–1054.

Young, L.J., Lim, M.M., Gingrich, B., and Insel, T.R. (2001). Cellular mechanisms of social attachment. Horm. Behav. *40*, 133–138.

Yuan, K., Shih, J.Y., Winer, J.A., and Schreiner, C.E. (2011). Functional networks of parvalbumin-immunoreactive neurons in cat auditory cortex. J. Neurosci. *31*, 13333–13342.

Cell

EXTENDED EXPERIMENTAL PROCEDURES

Cre Driver Lines

Tyrosine hydroxylase (TH)::IRES-Cre transgenic mice (EM:00254) were obtained from the European Mouse Mutant Archive. Mice were backcrossed at least 5 generations with C57BL6 wild-type mice prior to use. C57BL6J wild-type mice were obtained from Jax (SN: 000664). Tg(Drd1a-Cre)EY262Gsat were obtained from the Mutant Mouse Regional Resource Center at UC Davis (SN: 17264) and were also backcrossed with C57BL6 wild-type mice.

Viral Production

Complete maps of the viral constructs used are available online at http://www.optogenetics.org. AAV expression vectors were created by subcloning the entire DIO cassette into a modified version of the pAAV2-MCS vector, followed by recombinant AAV vector packaging and pseudotyping with AAV5 coat proteins (for DIO-ChR2, DIO-eNpHR3.0, DIO-EYFP, and DIO-OptoD1) or AAV2 coat proteins (for WGA-Cre) by the University of North Carolina (UNC) Chapel Hill Vector Core at titers of 3.0×10^{12} cfu ml^{-1} (ChR2), 2.0×10^{12} cfu ml^{-1} (Opto-D1), 1.5×10^{12} cfu ml^{-1} (eYFP), 3.0×10^{12} cfu ml^{-1} (WGA-Cre), and 3.0×10^{12} cfu ml^{-1} (eNpHR3.0).

Stereotaxic Virus Injection and Cannula Implantation

Animals were anesthetized with 2% isoflurane and placed in a stereotaxic head frame on a heat pad. Opthalmic ointment was applied to the eyes to prevent drying. A midline incision was made down the scalp and a craniotomy was made using a dental drill. A 10 μl Nanofil Hamilton syringe (WPI, Sarasota, FL) with a 34 gauge beveled metal needle was used to infuse virus with a microsyringe pump (UMP3; WPI, Sarasota, FL) and its controller (Micro4; WPI, Sarasota, FL). Virus was infused at a rate of 100 nl per min. Following infusion, the needle was kept at the injection site for 10 min and then slowly withdrawn. All stereotaxic coordinates are relative to bregma. TH::Cre mice were injected at two sites in the VTA (−3.3 mm anteroposterior (AP); 0.3 mm mediolateral (ML); −4.7 and −4.2 mm dorsoventral (DV)) with a total of 1.5 μl of virus. For VTA cell body stimulation, mice were implanted with a 200 μm diameter 0.22 NA mono fiber-optic cannula (Doric lenses, Quebec City, QC, Canada) directly above the VTA at −3.3 mm (AP); +0.3 mm (ML); −4.0 mm (DV). For stimulation of VTA-to-NAc projections, the optical fiber was unilaterally implanted over the medial shell of the NAc (+1.25 mm (AP); +0.75 mm (ML); −3.9 mm (DV)). For stimulation of VTA-to-PFC projections, a bilateral dual fiber-optic cannula (Doric lenses, Quebec City, QC, Canada) was implanted over the prelimbic region of the mPFC at +1.8 mm (AP); 0.35 mm (ML); −2.2 mm (DV). For pharmacological experiments, in addition to optical fiber placement above the VTA, a bilateral cannula (PlasticsOne, Roanoke, VA) was implanted above the medial shell of the NAc for infusion of dopamine receptor antagonists. Drd1::Cre mice were injected bilaterally with 1 μl of virus at a single site in the medial shell of the NAc at +1.25 mm (AP); 0.75 mm (ML); −4.5 mm (DV), and a dual fiber-optic cannula was implanted at the same coordinates used for stimulation of VTA-to-NAc projections. For trans-synaptic targeting experiments, wild-type mice were injected with 1 μl WGA-Cre virus in the medial shell of the NAc (same coordinates as Drd1::Cre injection) and 1.5 μl DIO-ChR2 virus in the VTA (same coordinates as TH::Cre injection), and optical fibers were placed at the same coordinates used for VTA cell body stimulation in TH::Cre mice. Cannulas were secured to the skull using a base layer of adhesive dental cement (C&B Metabond; Parkell, Edgewood, NY) followed by a second layer of cranioplastic cement (Ortho-Jet; Lang, Wheeling, IL). The incision was closed with sutures (Henry Schein) and animals were given a subcutaneous injection of buprenorphine (0.05 mg/kg) prior to recovery under a heat lamp. Behavioral experiments were conducted 4 weeks later for cell body stimulation, 8 weeks later for VTA-to-NAc projection stimulation, and 12 weeks later for VTA-to-PFC projection stimulation to allow for sufficient viral expression in axon terminals.

Viral injections of AAV5-DIO-EF1α-GCaMP5g in Th:Cre mice were identical to those used in the optogenetic experiments, but differed in the size (400 μm 0.48 NA) and placement (−3.3 (AP), 0.4 (ML), −4.2 (DV) for VTA cell bodies; +1.25 (AP), 0.75 (ML), −4.3 (DV) for VTA-to-NAc projections) of the fiber-optic cannula (Doric lenses, Quebec City, QC, Canada). VTA cell body and projection fiber photometry experiments were carried out at 4 weeks and 8 weeks after surgery, respectively.

Behavioral Analysis

Social Interaction Assay

Social interaction in the home cage was examined as described previously (Winslow, 2003). Briefly, cagemates were temporarily moved to a holding container and the test animal was connected to the fiber-optic patch-cord and allowed to explore its cage with the lid removed for 1 min. To ensure recruitment of DA signaling mechanisms throughout the social assay in a stable fashion, for the initial phasic VTA-DA ChR2 group optical stimulation was then delivered for 3 min prior to social interaction, and continued for 2 min after a stranger mouse (6-8 weeks) of the same sex and strain was placed into the test animal's home cage. Pretreatment in this fashion was not necessary and in subsequent groups the pre-stimulation period began immediately preceding introduction of the target. The two mice were allowed to freely interact and were video recorded with a camera suspended above the home cage. Social interaction over the 2 min of testing was manually scored later and defined as any period of time in which the test mouse was actively investigation the stranger mouse. Investigation included sniffing in active contact with the stranger's snout, flank, or anogenital area, grooming, or pursuing the stranger as it actively explored the cage; converse investigation of the test mouse by the stranger was not scored. Each mouse underwent two social interaction tests separated in time by one hour, with one stranger paired with

optical stimulation and one with no stimulation. Groups were counterbalanced for order of light stimulation and all behavior was scored blind to genotype.

Novel Object Investigation

The novel object test was performed in the home cage exactly like the social interaction assay, with either a plastic ball or wooden block (of equivalent size) introduced to the animal's home cage. Total time spent investigating the object was quantified over 2 min. Objects were thoroughly cleaned with soap and water in between tests to remove odor traces.

Sucrose Reward Assay

To investigate the fiber photometry signal of DA neurons in the VTA associated with reward, mice were placed in an operant chamber that was empty except for a single spout offering ad libitum access to sucrose water (10% by weight). Prior to testing, mice were water deprived for five days with access to 1 ml of water per day and ad libitum access to food. Individual trials in the operant chamber lasted 1 hr. Licks were detected using a contact lickometer, which relied on the electrical connection formed between the metal spout and the metal cage floor whenever a mouse made contact with the spout. The TTL signal from the lickometer was processed and time-locked through the same LabJack DAQ used to record fiber photometry data.

Open Field Test

To investigate the effects of optical stimulation on general locomotion, animals were individually placed in the periphery of the open field test chamber (50 cm x 50 cm) and were permitted to freely investigate the chamber during a 15 min session. The session was divided into three continuous 5 min epochs, with light delivered only during the 2nd epoch as described above. Total distance traveled was measured using video tracking software and compared between the light on epoch and average of the two light off epochs (Viewer 2, BiObserve, Ft. Lee, NJ).

Elevated Plus Maze

To investigate the effects of optical stimulation on anxiety-like behavior, animals were individually placed in the center of a plastic elevated plus maze consisting of two open arms (30 × 5 cm) and two closed arms (30 × 5 x 30 cm) extending from a center platform (5 × 5 cm). The maze stood 30 cm above floor level. Animals were permitted to freely investigate the maze during a 15 min session, divided into three continuous 5 min epochs, with light delivered only during the 2nd epoch as described above. The same video tracking software used for open field recordings was used to track the mouse's location and track length in closed versus open arms for the three epochs.

Conditioned Place Aversion

CPA was performed in a rectangular apparatus consisting of two side chambers measuring 28 × 24 cm each, and a center chamber measuring 11.5 × 24 cm. One side had black and white stripes on the walls with a metal grid floor, and the other had black and white squares on the walls with a punched metal floor. On Day 1 mice were allowed to explore the entire apparatus for 15 min. On days 2 and 3 mice were confined to one of the side chambers and optically stimulated for 30 min (counterbalanced for left or right chamber). On Day 4 mice were again allowed to freely explore the entire apparatus and preference for the stimulated chamber was compared to Day 1.

Home-Cage Behavioral Scoring for Fiber Photometry

For detailed analysis of target-related and solitary home-cage behaviors (Figure 1, 7), behavior during spliced video clips was assigned to one of the following categories: interaction, approach, withdrawal, ambulation, grooming, rest, burrowing, rearing, and head extension. Interaction was defined as sniffing at, or direct contact with, the target. Approach was defined as any time when the test mouse was moving its entire body (walking or running) toward the target but not yet in contact with or sniffing it. Withdrawal was defined as any time when the test mouse moved its entire body away from the target. Ambulation was defined as any walking or running around the home cage not related to approach or interaction with the target. Grooming was defined as sitting stationary while using the forelimbs or mouth to clean the snout or flank. Rest was defined as the animal sitting still in one location and not moving at all. Burrowing was defined as moving forward while using the snout and forelimbs to shovel bedding aside. Rearing included any time when the animal was standing only on its two hind limbs, or leaning against the side of the home cage. Head extension was defined as any period in which the mouse's body was stationary but it was moving its head around, not directed at the target.

Chimeric Opto-D1 Receptor Construction

Mammalian codon-optimized sequences of Opto-D1 (design approach as previously described (Airan et al., 2009); amino acid sequences in Figure S4) were synthesized (DNA2.0), cloned into pcDNA3.1 and fused to the N terminus of YFP (with START codon deleted) using NotI.

In Vitro GPCR Signaling Assays

HEK293FT cells (Invitrogen) were transfected using Lipofectamine 2000 (Invitrogen) in 24-well plates and changed to serum-free medium 4-6 hr post-transfection. Approximately 24 hr post-transfection, 1 μM all-trans retinal (ATR) was added and plates were transferred to the stage of a microscope within an environmentally controlled chamber (Leica DMI6000; 37C, 5% atmospheric CO2). 5 regions/well were optically stimulated for 1 min each (Sutter 300W Lambda DG-4; Semrock 504/12nm bandpass filter; 10x 0.3NA objective). Following a 20 min incubation, cells were lysed and analyzed by HTRF (CisBio) and a Biotek Synergy4 reader.

Immunohistochemistry and Confocal Microscopy

For cFos quantification, mice were optically stimulated in their home cage for 5 min (with the same stimulation protocol used for behavioral testing) 90 min prior to sacrifice. For all cohorts, animals were anesthetized and transcardially perfused with ice-cold 1X PBS followed by 4% paraformaldehyde (PFA) in PBS. Brains were post-fixed for 48 hr in 4% PFA and then placed for at least 24 hr at 4°C in a 30% sucrose solution in PBS until settling. Brains were sectioned into 40 μm thick slices using a freezing microtome and stored in cryoprotectant at 4°C in the dark until antibody staining. Free-floating sections were washed 3 × 10 min in PBS and then blocked for 1 hr in 0.3% TritonX and 3% normal donkey serum (NDS). Primary antibody incubations (rabbit anti-cFos 1:500, Calbiochem, La Jolla, CA; chicken anti-tyrosine hydroxylase (TH) 1:500, Aves Labs, Tigard, OR) were performed overnight at 4°C in 3% NDS/PBS. Sections were then washed 5 × 10 min and incubated with secondary antibodies (Cy3 donkey anti-rabbit and Cy5 donkey anti-chicken; both 1:1000, Jackson Laboratories, West Grove, PA) for 3 hr at room temperature. Slices were washed 2 × 10 min in PBS, 1 × 10 min in 1:50,000 DAPI, 1 × 10 min in PBS and mounted on microscope slides with PVA-DABCO. Images were acquired on a Leica TCS SP5 scanning laser microscope. Counting of cFos-positive cells was done on z-stacks of the entire slice volume by an observer blind to experimental condition.

Behavioral Pharmacology

A 26-gauge stainless steel bilateral internal cannula (PlasticsOne) projecting 0.5 mm beyond the tip of the guide cannula was connected to a micro-syringe pump by a PE20 tube. D1 antagonist, D2 antagonist, or saline were infused in a volume of 0.4 μl at a rate of 100 nl/min. The internal cannula was withdrawn 2 min after infusion finished and animals underwent social testing 10 min following drug infusion. Testing took place over 4 days, and each day an individual animal received only one drug ± light, counter-balanced for treatment order. For D1 receptor antagonism, SCH23390 was infused 400 ng/0.4 μl per side at a concentration of 3.1 mM. For D2 receptor antagonism, raclopride was infused 400 ng/0.4 μl per side at a concentration of 2.89 mM.

In Vivo Electrophysiology

Optrode Recordings in Anesthetized Animals

Simultaneous optical stimulation and electrical recording in the VTA/ NAc of TH::Cre ChR2 mice was performed as previously described (Gradinaru et al., 2007). Animals were anesthetized with 2% isoflurane and placed in a stereotaxic frame. Extracellular tungsten electrodes (Catalog #573220, A-M systems) were glued to a 0.37 NA 200 μm diameter optical fiber (Thorlabs) such that the electrode tip extended ~500 μm deeper than the fiber tip. Optrodes were stereotaxically lowered into the VTA (−3.3 mm (AP); 0.3 mm (ML); −4.2 mm (DV)) and NAc (+1.25mm (AP); +0.75 mm (ML); −3.9 mm (DV)) for simultaneous VTA stimulation and recording in both VTA and NAc. Isoflurane levels were reduced to 1% prior to acquiring recordings. NAc optrodes were advanced in 50 μm increments and recordings were taken along the full dorsoventral axis of the medial NAc in response to VTA stimulation. To analyze the NAc multiunit response evoked by VTA stimulation, a single phasic burst (8 5-ms pulses delivered at 30 Hz) of light was delivered to the VTA, and simultaneous 10 s recordings were taken in VTA and NAc.

Clampex software (Molecular Devices, Sunnyvale, CA) was used for recording extracellular signals as well as for controlling a 473 nm diode-pumped solid state laser (OEM Laser Systems). Light power measured from the tip of the optical fiber was 10 mW, giving a predicted irradiance of 10 mW/mm^2 at the recording site 500 μm from the fiber tip (Aravanis et al., 2007). Extracellular signals were bandpass-filtered between 600 and 6000 Hz and digitized at 32 kHz. Spikes were isolated using custom Matlab software with the threshold for event detection set at 5 standard deviations above the mean. To quantify the NAc response, firing rates were calculated during 4 s of pre-stimulation baseline, during stimulation (0.23 s), and during the 4 s following stimulation. Error bars represent SEM calculated across 25 recording sites from 2 animals, each with 3 stimulation trials (all recording sites were included in analysis with no pre-selection of responsive sites). For Opto-D1 mice, a single optrode was lowered into the NAc and a single continuous 8 s pulse of blue light was delivered at each recording site. Recordings were obtained in 47 sites from 2 animals, each with 4 stimulation epochs.

Multielectrode Recordings in Behaving Animals

TH::Cre mice were injected with DIO-ChR2 virus and implanted with an optical fiber in the VTA as described above. A custom-made fixed bundle electrode (NB Labs, Denison, TX) comprised of 16 50-μm Teflon stainless steel wires attached to a nano strip connector (Omnetics) was targeted to the medial shell of the NAc. A silver ground wire was inserted into a small craniotomy above cortex immediately anterior to the cerebellum. Mice were allowed to recover for four weeks before recording. Electrical signals were digitized using Neuralynx Digital Cheetah. Multiunit activity was recorded at 32 kHz, bandpass filtered (300-10000 Hz) and events that exceeded a threshold of 40 μV were classified as spikes. Videos and laser pulses were recorded with Neuralynx Cheetah software and synchronized with the neural recording. The animal's movement was tracked using a headstage LED in a dimly lit environment.

For several days prior to beginning recording, animals were acclimated to having the Neuralynx headstage and optical fiber plugged in. Awake recordings of the effect of VTA stimulation on NAc activity were performed in the animal's home cage. Recordings lasted 20-30 min with 1 min long phasic stimulation epochs (same stimuli as used for behavior) separated by 2 min of no light. To study NAc spiking activity in a mouse engaging in social interaction, recordings were performed in a three-chamber social interaction environment in order to have clearly defined social and non-social zones with which to correlate NAc activity (Moy et al., 2004). Implanted mice were placed in the center chamber of the three-chamber apparatus with the two side chambers closed off and allowed to acclimate for 10 min. In one side chamber designated the "social chamber," a stranger mouse was placed inside a small

wire cage in one corner (Galaxy pencil cup, Spectrum Diversified Designs). The ''neutral chamber'' contained an identical but empty wire cage.

Electrical and video tracking recordings began when the doors to the two chambers were removed and animals were allowed to freely explore the entire apparatus for 20 min without any stimulation. Recordings were obtained from 41 different sites in 3 animals. Events larger than 3 standard deviations from the mean were used for multiunit activity analysis. To calculate firing rate heat maps, two matrices were generated for each multiunit recording. The first matrix was a spike map which contained the number of spikes that occurred in each pixel of the environment, and the second matrix was a behavior map with the amount of time spent in each pixel. The spike map from each electrode was divided by the total number of spikes in that matrix. This creates a normalized spike map, and ensures that the final average result is not dominated by the recordings with more spikes. The normalized spike maps from all the recordings were then added to each other. The same was done with all the behavior maps. This summed spike matrix was then divided by the summed behavior matrix, creating an average firing rate map of all the multiunit recordings. The average firing rate map was smoothed using a cosine taper. To quantify the difference in firing rate across chambers, the fold-change in absolute firing rate between chambers was calculated for each recording site and significance was assessed using a paired non-parametric Wilcoxon's signed-rank test.

Fiber Photometry

Signals were collected at a sampling frequency of 250 Hz. Fluorescence signal was normalized within each mouse by calculating the dF/F as (F - median(F)) / median(F), where the median was taken over the entire behavioral trial. The lock-in amplifier increases the sensitivity of detection by attenuating any signal that is not modulated at a chosen frequency. By selectively modulating the fluorescence excitation laser with an optical chopper at a frequency of around 400 Hz, and connecting the output signal from the chopper with the sync input of the lock-in amplifier, it is possible to detect small fluorescence signals with no background noise - even in a fully lit room. Use of the chopper also opens up the possibility of simultaneous optogenetic stimulation through the same fiber with minimal cross-talk in the fluorescence signal by using an un-chopped stimulation laser and a red-shifted opsin. Because the lock-in amplifier relies on temporal averaging to clean up the signal, there is a tradeoff between the effective sampling period (around 5 times the lock-in time constant) and the amount of noise in the signal. We found that a time constant as short as 3 ms yielded a good signal. The custom software freely available on request provides a simple interface for viewing and recording data from the Labjack DAQ, including the ability to synchronize fluorescence data with other signals such as lickometer timestamps, and timestamps of a flashing LED that is visible in the behavioral videos. Data acquisition and analysis code can also be obtained at https://github.com/logang/Fiberkontrol.

Statistical Analysis

Hypotheses involving more than two group means were tested using linear contrasts in a linear mixed effects (LME) model (using restricted maximum likelihood criterion in the 'lmer' package in R) and with confidence intervals for fits generated using 1000 Markov-Chain Monte Carlo samples from the posterior of the parameters. All hypothesis tests were specified a priori. Subjects were modeled as random effects in LME models. For latency analysis, to avoid over-fitting, we cross-validated across animals (n = 10), leaving one animal out of each fit and using this animal to estimate prediction error (repeating this for all animals). As Kaplan-Meier estimates of survival probability used to compare latency to interact looked very similar within animals (for social and novel conditions) we combined observations across animals within condition (social or novel), and used a log-rank test to test if the groups showed significantly different group survival curves. For survival regression, Ca^{2+} data was log-transformed, as this transformation rendered them unimodal and approximately Gaussian (consistent with model assumptions), and random effects included to account for animal-specific effects. No animal-specific effects were significant in the regressions after a Holm's step down procedure for controlling family-wise error rate, consistent with the observed similarity in KM estimates. Our causal mediation analyses are similar in character to the standard examples for continuous covariates and treatment given in the library documentation. In particular we use survival regression for the outcome model, a linear regression for the mediator model, and again both regressions include random effects to account for differences between individual animals.

Peaks in the fiber photometry data were identified using the following efficient heuristic: 1) take the derivative of the squared difference between two different low pass filtered copies of the time series data (at 40Hz and 0.4Hz); 2) threshold these values at 2.91 times the median absolute deviation (MAD) of the resulting time series (the approximate 95% confidence interval MAD estimate for Gaussian data); 3) classify these smooth derivative-based time points as ''peaks'' if absolute fluorescence measurement is above 2.91*MAD of the fluorescence intensity. Note that as expression levels and fiber placement differed among animals, all calculation of thresholds was done within animal. Smoothed behavior plots (Figure 7) were made using the same adaptive smoothing kernel density estimation algorithm (''akj'' in the R ''quantreg'' library) as used for firing rate estimation, and plotted using the d3.js library. All binary comparisons in Figure 7 were corrected using a Holm step down procedure with ''p.adjust'' in R.

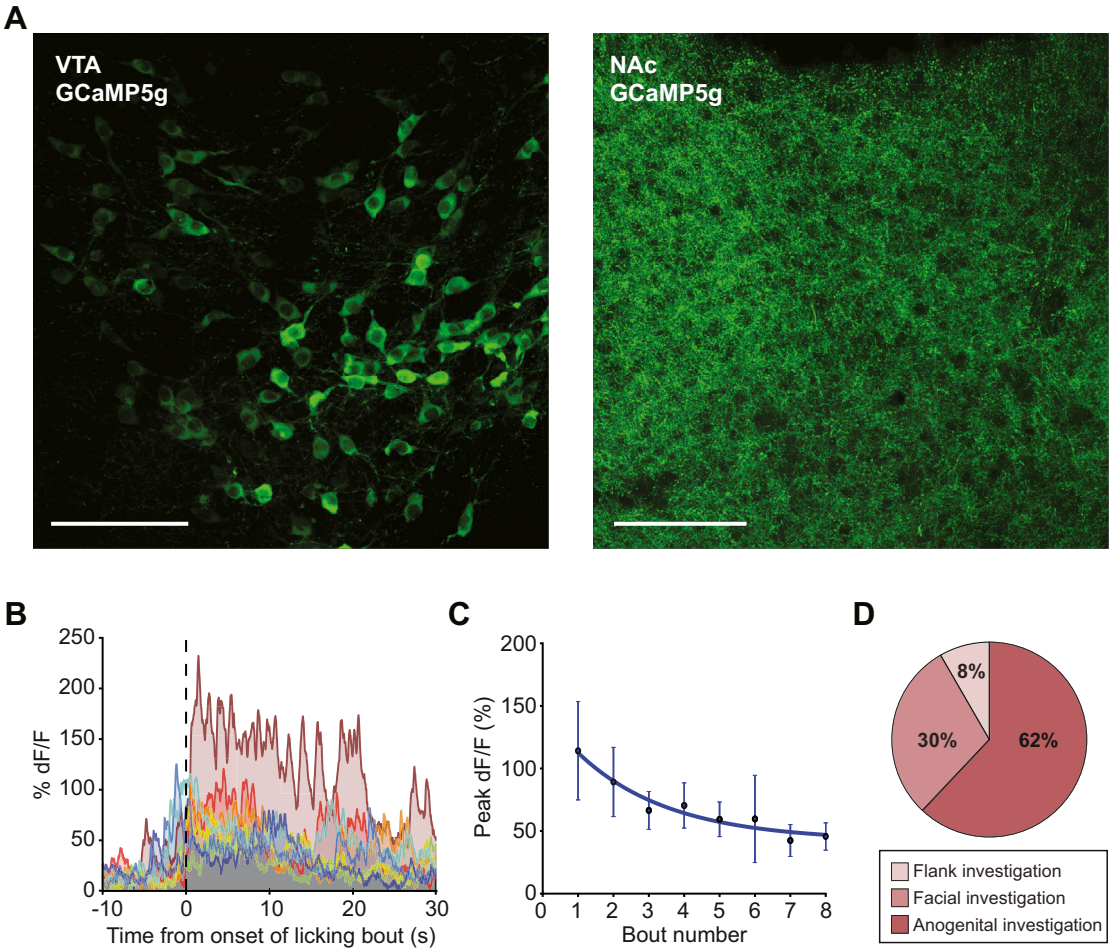

Figure S1. Related to Figure 1

(A) Confocal images showing TH-GCaMP5g expression in VTA cell bodies (left) and in VTA-NAc axons (right). Scale bar represents 100 μm.

(B) Example peri-event plot showing changes in fluorescence aligned to the start of each licking epoch. Warmer colors indicate earlier licking epochs; cooler colors indicate later epochs.

(C) Plot of average peak fluorescence recorded across bouts, indicating a decay of the signal over time.

(D) Refined analysis of subtypes of social interaction during peak fluorescence (from Figure 1I).

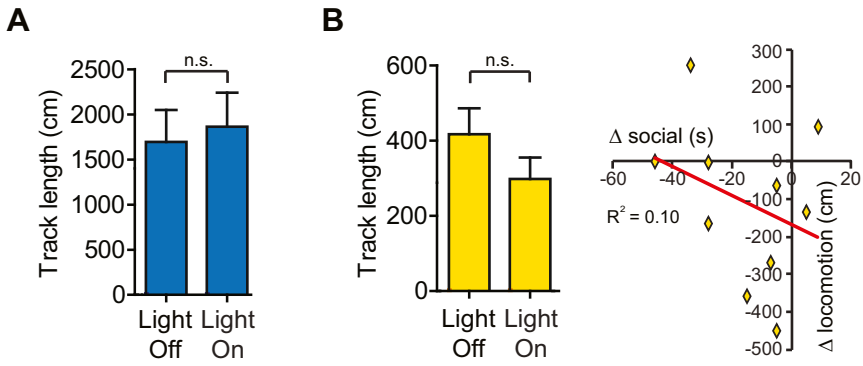

Figure S2. Related to Figure 2

(A) VTA stimulation had no significant effect on open field track length (n = 17, Wilcoxon signed-rank test, p = 0.85).

(B) Left: VTA inhibition had no significant effect on open field track length (n = 10, Wilcoxon signed-rank test, p = 0.16). Right: plot of change in social interaction versus change in locomotion, showing no positive correlation.

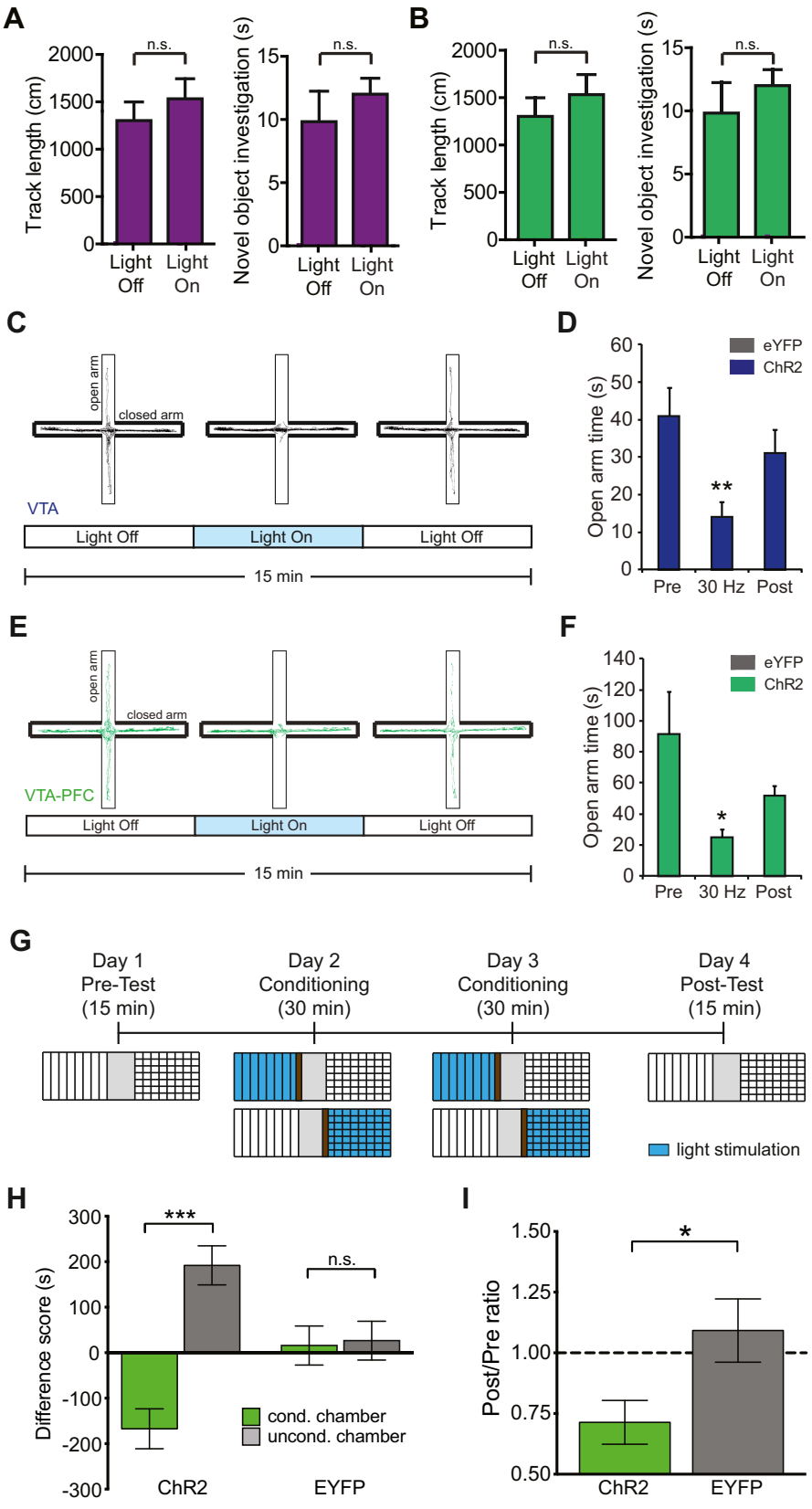

(legend on next page)

Figure S3. Related to Figure 4

(A) Left: VTA-NAc projection stimulation had no effect on open field track length (n = 12, Wilcoxon signed-rank test, p = 0.62). Right: VTA-NAc projection stimulation had no effect on novel object investigation (n = 12, Wilcoxon signed-rank test, p = 0.63).

(B) Left: VTA-PFC projection stimulation had no effect on open field track length (n = 7, Wilcoxon signed-rank test, p > 0.05). Right: VTA-PFC projection stimulation had no effect on novel object investigation (n = 7, Wilcoxon signed-rank test, p = 0.16).

(C) Representative trace of one VTA-ChR2 animal track during a 15 min exposure to the EPM. Open-arm exploration acutely decreased during the VTA cell body stimulation epoch (middle).

(D) Summary of anxiogenic effect of VTA stimulation expressed as light-evoked change in open arm time. Blue: ChR2, gray: eYFP controls (n = 12 ChR2, n = 12 eYFP, p = 0.01).

(E) Representative trace of one VTA-PFC ChR2 track in the EPM, showing an acute decrease in open arm time during VTA-PFC projection stimulation.

(F) Phasic stimulation of VTA axons in PFC acutely and reversibly decreased open arm time in the in ChR2 mice (green) but not controls (gray; n = 7 ChR2 and n = 7 eYFP, p = 0.02).

(G) Schematic of conditioned place aversion paradigm. Mice were conditioned for two days by being confined to one side of the apparatus for 30 min paired with stimulation.

(H) Summary of aversive effect of VTA-PFC projection stimulation represented as difference in time spent in each chamber before and after two days of conditioning (n = 12 ChR2 and n = 14 eYFP, Mann Whitney test, p = 0.0001).

(I) Data from (H) represented as the ratio of time spent in the conditioned chamber pre- versus post-conditioning (n = 12 ChR2 and n = 14 eYFP, Mann Whitney test, p = 0.02).

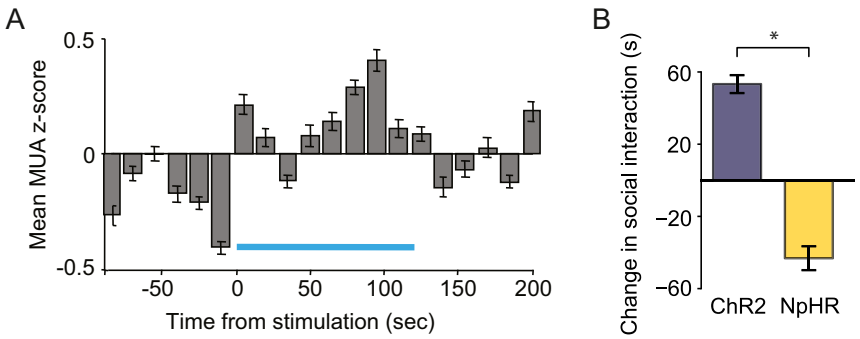

Figure S4. Related to Figure 5

(A) Average multiunit activity in NAc before, during, and after phasic VTA stimulation recorded from awake animals alone in their home cage. Blue bar: delivery of eight 5 msec pulses of 30 Hz phasic bursts of light every 5 s for a total of 2 min. Recordings were taken for 20 min with alternating 2 min intermittent epochs of phasic stimulation and averaged to make the PSTH (n = 41 recording sites, Wilcoxon signed-rank test, $p < 0.05$).

(B) Light-evoked change in social interaction measured as time spent in the social side of a three-chamber apparatus, showing similar bidirectional effects on social behavior as the home cage assay with stimulation of D1 cells or inhibition of VTA-DA cells (n = 6 ChR2 and n = 10 NpHR, LME model, $t_{23} = 2.32$, $p = 0.03$).

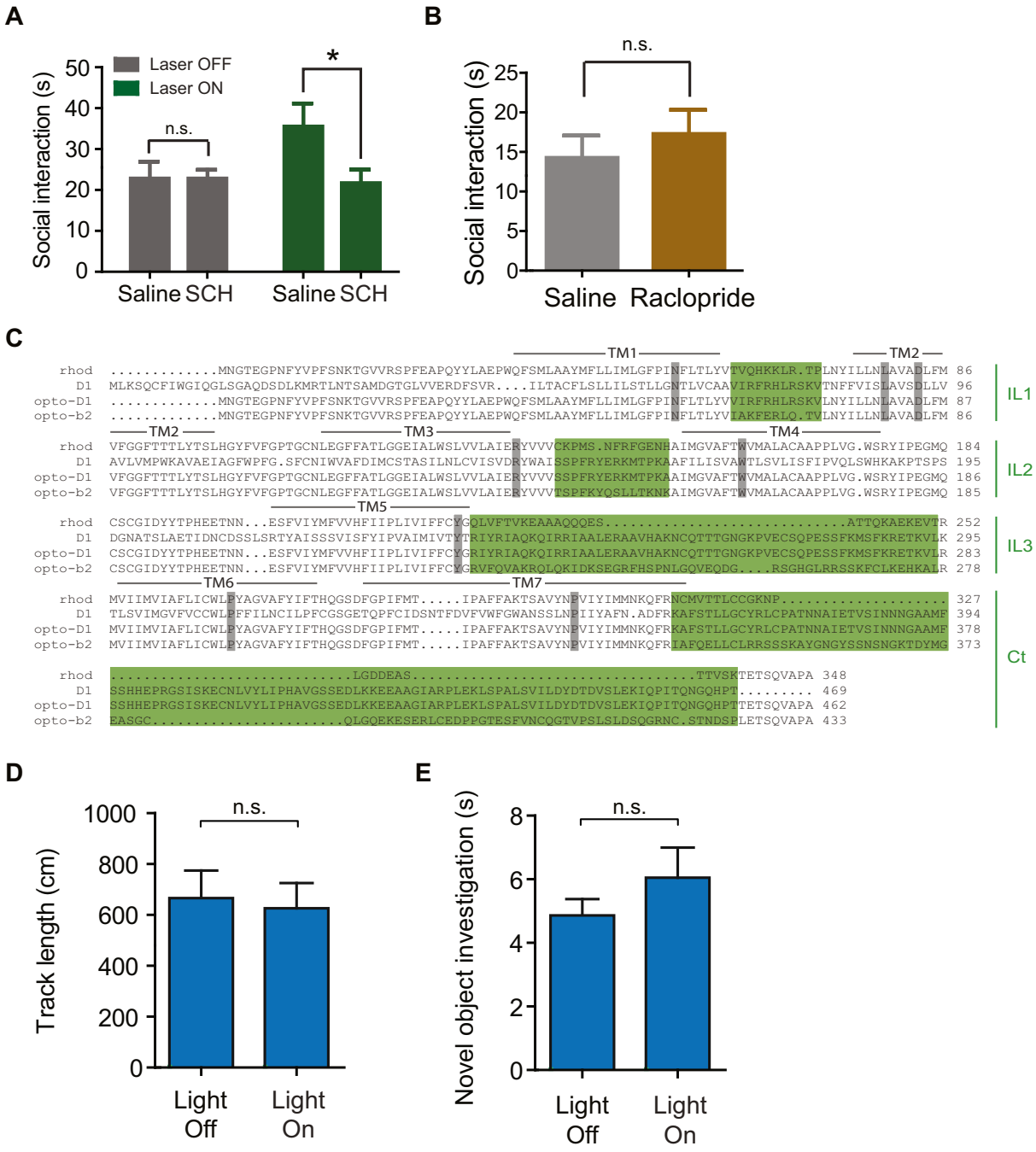

Figure S5. Related to Figure 8

(A) D1 antagonism (SCH) data from Figure 8B presented as time spent engaging in social interaction across 4 groups (no stimulation + saline, no stimulation + SCH, VTA stimulation + saline, and VTA stimulation + SCH) to illustrate the observation that SCH blocks the stimulation-evoked increase in social behavior but does not affect basal levels of social interaction (n = 15, LME model, $t_{18} = 2.29$, p = 0.035).

(B) The D2 receptor antagonist raclopride had no significant effect on social interaction during VTA stimulation (n = 15, Wilcoxon signed-rank test, p = 0.49).

(C) Primary structure alignment of wild-type G protein-coupled receptors (Rhodopsin (rhod) and D1 receptor) and OptoXRs (Opto-D1 receptor, previously-published Opto-β_2 adrenergic receptor). Gray: highly conserved residues; green: swapped intracellular domains (IL, intracellular loop; Ct, C terminus; TM, transmembrane domains).

(D) Opto-D1 activation in NAc had no effect on open field track length (n = 19, Wilcoxon signed-rank test, p = 0.52).

(E) Opto-D1 activation in NAc also had no effect on novel object investigation (n = 17, Wilcoxon signed-rank test, p = 0.39).